MANY BODY INTERACTIONS: PART ONE. INTERACTIONS BETWEEN SOLUTE MOLECULES IN LIQUID ARGON; PART TWO. THE INTERACTION BETWEEN KRYPTON AND THE (1, 1, 0) FACE OF COPPER SINGLE CRYSTALS

A THESIS

Presented to

The Faculty of the Division

of Graduate Studies

by

Stephen Laurent Parrott

In Partial Fulfillment

of the Requirements for the Degree

Doctor of Philosophy

in the School of Chemistry

Georgia Institute of Technology

June, 1977

MANY BODY INTERACTIONS: PART ONE. INTERACTIONS BETWEEN SOLUTE MOLECULES IN LIQUID ARGON; PART TWO. THE INTERACTION BETWEEN KRYPTON AND THE (1, 1, 0) FACE OF COPPER SINGLE CRYSTALS

Approved:

Robert A. Pierotti, Chairman

T. F. Moran

E. J. Schiebner

Date approved by Chairman: 6 June 1977

ACKNOWLEDGEMENTS

The author wishes to thank all of those who aided him in the course of this work.

Special thanks are warmly given to Dr. Robert A. Pierotti, who suggested these problems, and who offered the much needed advice and encouragement necessary to complete these studies.

Thanks are also given to Dr. W. R. Livesay of the Georgia Tech Engineering Experiment Station for the use of the special apparatus needed for the growth of the copper crystals, and to Russell E. Eibling, who put the apparatus in working order and grew several of the crystals used in this study.

The author has also greatly appreciated the help and advice given to him by Dr. Albert A. Liabastre and Chia Chi Yang; he also would like to thank Dr. E. J. Schiebner and Dr. T. F. Moran for their helpful suggestions regarding the content of this manuscript.

Thanks are also due for the technical help of Kenneth Williams, Donald Lillie, and Gerald O'Brien.

The financial help of his parents, Neil and Barbara, is gratefully acknowledged.

Finally, the author wishes to offer special thanks to his wife Cheri', who not only offered vital encouragement, but who also cheerfully typed this manuscript twice.

TABLE OF CONTENTS

LIST OF TABLES

Table Page

LIST OF ILLUSTRATIONS

LIST OF SYMBOLS (PART ONE)

A = Helmholtz free energy (except equation (I-101))

a = activity (or distance, as in equation (I-102)-(I-107) and figures 5 and 6)

B = virial coefficient for molecules in dilute gases; see equations (I-36)-(I-37)

B^* = virial coefficient for molecules in liquid phase

b = terms in the series equation (I-18), related to B by equations (I-26)-(I-27)

b_0 = $(2/3)\pi N_0 \sigma^3$, used in finding B (equation (I-98))

E = energy

f = fugacity

G = free energy

$g(r)$ = radial distribution function

K_H = Henry's Law Constant

k = Boltzmann constant

m = N_2/N_1

N = number of molecules

N_0 = Avogadro's number

P = total hydrostatic pressure

Q = canonical ensemble partition function

R = gas constant

r = distance between molecular centers

R = σ_2/σ_1

S = entropy

T = absolute temperature

U = potential energy

V = volume

W = work required to dissolve the solute

X = integrals related to B^* (see equation (I-75))

x = mole fraction (or distance, as in equations (I-102)-(I-107), and figures 5 and 6)

Z = configuration integral, given by equation (I-35)

z = an activity, f/kT

Greek Letters

β = isothermal compressibility

Γ = semi-grand, isobaric, isothermal partition function

γ = activity coefficient, $\gamma = a_2/x_2$

γ' = activity coefficient, $\gamma' = a_2/m_2$

Δ = isobaric, isothermal partition function

δ = coefficients in the series equation (I-56); or a numerical fraction of W (equation (I-111))

ε = interaction energy term in Lennard-Jones (6-12) potential function

ε^* = an effective interaction energy

Θ = coefficients in the series equation (I-49)

Λ = de Broglie thermal wavelength

λ = absolute activity = $e^{\mu/kT}$

μ = the chemical potential

Ξ = the grand canonical partition function

ξ = a pairwise potential function (equation (I-90))

ρ = number density

σ = molecular diameter as used in the Lennard-Jones (6-12) potential function

Ω = microcanonical ensemble partition function

Subscripts

1 = refers to component one, the solvent

2 = refers to component two, the solute

c = cavity term in the scaled particle theory

i = interaction term in the scaled particle theory; counting indes in some series

j = counting index in some series

k = counting index in some series

Note: except for equations (I-102)-(I-107), a double subscript AB, such as Q_{AB}, is used to indicate A molecules of component one (the solvent) and B molecules of component two (the solute).

Superscripts

G = refers to properties of the gas phase

L = refers to properties of the liquid phase

∞ = the value at infinite dilution

Note: a bar over a quantity indicates it is a molar quantity.

SUMMARY - PART ONE

A mathematical relationship is developed which allows information about solute-solute interactions to be obtained from phase equilibrium data. It is assumed that solute behavior can be analyzed by a virial type expansion, and that the resulting virial coefficients are a reflection of the potential of average force which influence the solute behavior. Published data on the He-Ar,[1,2] Ne-Ar,[3] and H_2-Ar[4] systems were analyzed by this method, thus obtaining second virial interaction coefficients, B_2^*, at various temperatures for the solute pairs He-He, Ne-Ne, and H_2-H_2 when these are immersed in a liquid Ar medium. The values of B_2^* for He ranged from -239 cm^3/mole at 93.2°K to -12 cm^3/mole at 148.2°K; the values for Ne ranged from -62 cm^3/mole at 84.42°K to -28 cm^3/mole at 129.93°K; and those for H_2 ranged from -16 cm^3/mole at 94.2°K to +7 cm^3/mole at 140°K.

For the purpose of providing a physical interpretation to the experimental results, a simple model of solute interactions is presented. The results based on this model show that as a result of bringing two solute molecules together, in effect two solvent molecules also become associated and two solute-solvent pairs become separated.

A second virial coefficient is obtained by integrating an effective solute-solute potential which also includes these changes in solvent interactions; from 85° to 140°K these coefficients range from -150 to -58 cm^3/mole for He, from -73 to -24 cm^3/mole for Ne, and from -47

to -10 cm^3/mole for H_2.

Finally, experimental results are incorporated into the model calculations. From 85° to 140°K, the resulting virial coefficients range from -290 to -24 cm^3/mole for He, from -51 to +30 cm^3/mole for Ne, and from -33 to +17 cm^3/mole for H_2. In this instance, one adjustable parameter was used; however, its value was the same for each solute.

SUMMARY - PART TWO

The interaction of krypton with a copper (1, 1, 0) surface was investigated. Adsorption isotherms were measured at 72.8°, 79.9°, 92.2°, 101.6°, and 108.1°K. These were analyzed by a virial treatment, which yielded a gas-solid interaction parameter $\epsilon'_{ls}/k = 1672°K$. These results were compared with a previous work on the krypton adsorption on copper (1, 1, 1) crystals. Evidence that the structure of the (1, 1, 0) surface has influenced the adsorption behavior is also presented.

Potential curves for the interaction of krypton with the (1, 1, 1) and (1, 1, 0) face of copper were calculated by assuming the metal to be a lattice network of atoms which are 4.05 Å in diameter, but spaced 2.55 Å apart. The calculation predicts different interaction energies over different areas of the (1, 1, 0) surface; the highest energy is nearly equal to the interaction predicted for the (1, 1, 1) face.

PART ONE

INTERACTIONS BETWEEN SOLUTE MOLECULES IN LIQUID ARGON

CHAPTER I

INTRODUCTION

Just as intermolecular forces in a gas are responsible for liquid formation, so too are the physical forces between molecules in solution responsible for particular protein conformations, various enzymatic reactions, and so on. Understanding such complex problems as these, or simpler problems such as the effect of concentration on solubility, requires an understanding of these forces, and some theoretical progress has been made in this area.

Some of the previous theoretical work in this area has considered that the effect of the presence of a third polarizable body is to decrease the interaction energy of the other two bodies.[5] This gives a potential function for solute molecules that resembles the potential function between the same molecules in the gas phase, but reduced by some fraction. For example, calculations based on this idea show that the interaction energy between two carbon tetrachloride molecules is reduced 17% from the gas phase value when these are present in liquid benzene.[6]

The goal of this work was to obtain some information about solute interactions by analyzing phase equilibrium data. The analysis assumes that the dilute solution obeys Henry's Law, in analogy with dilute gases obeying the ideal gas law. At higher concentrations, deviations from Henry's Law arise as a result of the interaction between solute mole-

cules; then it is assumed that the solubility behavior can be described by some power series in the concentration. This is in analogy with the virial expansion for a gas, which is a power series in the gas density.

The virial coefficients, evaluated in either case by an analysis of deviations from ideal behavior, are functions of the forces that act between the molecules in either phase. From the theoretical considerations that were just discussed, it would appear that a comparison between the second virial coefficients for molecules in solution and the same molecules in the gas phase would reflect a decreased attractive force in solution.

CHAPTER II

THEORETICAL

This section will present the relations which are necessary to obtain the second virial coefficient for solute molecules, B_2^*, from phase equilibrium data. A thermodynamic relation will first show that deviations from ideal solubility behavior are contained in the activity coefficient, γ. Statistical mechanics will then relate certain molecular parameters of the solvent and solute to this activity coefficient, thus connecting solute interactions to solubility behavior. This treatment will require knowledge of the partial molar volume of the solute, which will be obtained from the scaled particle theory, and the fugacity of the solute, which can be calculated from the experimental data.

Solution Thermodynamics

If a particular component of a binary mixture is at equilibrium between the gas and liquid phases, (G and L, respectively), then its chemical potential in those phases must be equal.[7] Labelling the solute as component 2, then

$$\mu_2^G = \mu_2^L \qquad \text{(I-1)}^*$$

The chemical potential of component 2 in the gas phase is given by

*Equation numbers in Part One will be preceeded by Roman numeral I.

$$\mu_2^G = \mu_2^{G*}(T) + RT\ln f_2 \qquad (I\text{-}2)$$

where f_2 is the fugacity of the solute, $\mu_2^{G*}(T)$ is the chemical potential of an ideal gas at one atmosphere pressure, R is the gas constant and T is the absolute temperature. Similarly,

$$\mu_2^L = \mu_2^{L*}(P, T) + RT\ln a_2 \qquad (I\text{-}3)$$

where $\mu_2^{L*}(P, T)$ is the chemical potential of the solute referred to infinite dilution and a_2 is the activity defined by

$$a_2 = x_2\gamma_2 \qquad (I\text{-}4)$$

Combining these relations yields

$$\ln f_2/x_2 = \ln \gamma_2 + [\mu_2^{L*}(P, T) - \mu_2^{G*}(T)]/RT \qquad (I\text{-}5)$$

For infinitely dilute solutions, the quantity f_2/x_2 is known as the Henry's Law constant. Noting that

$$(\partial\mu_2^{G*}(T)/\partial P)_T = 0 \qquad (I\text{-}6)$$

and

$$(\partial\mu_2^{L*}(P, T)/\partial P)_T = \bar{V}_2^{\infty} \qquad (I\text{-}7)$$

where $\bar{V}_2^{\infty}$ is the partial molar volume of the solute at infinite dilution, the pressure derivative of equation (I-5) is then

$$[(\partial \ln f_2/x_2)/\partial P]_{T,x_2} = [\partial \ln \gamma_2/\partial P]_{T,x_2} + \bar{V}_2^{\infty}/RT \qquad \text{(I-8)}$$

In the experimental phase equilibrium studies, the liquid composition and total hydrostatic pressure are both changing. The value of γ_2 depends on composition, so that $\ln f_2/x_2$ varies with both composition and pressure. It is the compositional dependence which is to be extracted from the experimental data.

The Fugacity

An expression for the fugacity can be found from statistical mechanical consideration.[8] Consider first the microcanonical ensemble for a binary mixture: a large number, Ω, of systems, each with the same number of molecules of components one and two, N_1 and N_2, the same volume, V, and the same energy, E. The familiar procedure is to allow these systems to exchange energy (the total energy is constant) with one another, but V, N_1, and N_2 of each system remains constant; this collection of systems is called a canonical ensemble. At equilibrium, the Boltzmann distribution of energy levels is the most likely distribution. The sum over all energy states of the product of the number of states with energy E_i times the Boltzmann weighting factor $e^{-E_i/kT}$ is called the canonical ensemble partition function, Q:

$$Q(N_1, N_2, V, T) = \sum_{E_i} \Omega_{E_i}(N_1, N_2, V) e^{-E_i/kT} \qquad \text{(I-9)}$$

where k is the Boltzmann constant and T is the temperature.

This partition function then represents the sum over all accessible energy states of a system with a specified N_1, N_2, V, and T, and therefore represents a closed, isothermal system at constant volume. The Helmholtz free energy A is the characteristic thermodynamic function under these conditions; a comparison between statistical mechanical and thermodynamical equations leads to the relation

$$Q(N_1, N_2, V, T) = e^{-A(N_1, N_2, V, T)/kT} \qquad \text{(I-10)}$$

Unfortunately, the constraint that N_1 and N_2 be fixed is not particularly convenient to apply to gases, since density fluctuations do occur. We must then sum over various canonical ensembles, each containing different numbers of molecules N_1 and N_2, but all are at the same temperature and volume as before. The molecules will distribute according to their free energy, and the Boltzmann factor is therefore $e^{N\mu/kT}$, where N is the number of molecules of either component, and μ is the chemical potential of that component.

Proceeding as before,

$$\Xi(\lambda_1, \lambda_2, V, T) = \sum_{N_1, N_2 \geq 0} Q_{N_1 N_2}(V, T)\lambda_1^{N_1}\lambda_2^{N_2} \qquad \text{(I-11)}$$

where $\lambda = e^{\mu/kT}$ is the absolute activity and Ξ is the grand canonical partition function, which represents the sum of the accessible energy states for each accessible configuration of all of the molecules. The

fixed variables are the volume, temperature, and activities of the components, so that Ξ is representative of an open, isothermal system at constant volume.

By comparing related statistical mechanical and thermodynamic equations, it is found that

$$PV = kT\ln\Xi(V, T, \mu) \tag{I-12}$$

Another relation to thermodynamics which will prove useful later is

$$\bar{N} = kT(\partial \ln\Xi/\partial\mu)_{V, T} \tag{I-13}$$

Now, in order to relate molecular interactions with macroscopic gas behavior, first define

$$z_1 = Q_{10}\lambda_1/V \tag{I-14}$$

$$z_2 = Q_{01}\lambda_2/V \tag{I-15}$$

where, for example, Q_{10} represents a summation over energy states for a collection of systems of volume V, each containing one molecule of component one. The energy levels of the particle may then be described by the standard particle-in-a-box treatment of quantum mechanics. This ensemble resembles an ideal gas, and z_1 turns out to be the ideal gas density of component one at low gas densities.

Next, define

$$Z_{N_1N_2}/N_1!N_2! = Q_{N_1N_2} V^{N_1 + N_2} / Q_{10}^{N_1} Q_{01}^{N_2} \qquad \text{(I-16)}$$

where the $Z_{N_1N_2}$ are configuration integrals (quantitatively defined later); these represent sums over the energy states that arise as a result of the configurationally dependent energy of molecular interactions.

A pair of attractive molecules have more accessible energy states than a similarly positioned pair of non-interacting molecules; attractive molecules are then more likely to assume close together configurations. It is then the function of the $Z_{N_1N_2}$ to correct the ideal gas density based on the interactions of $N_1 + N_2$ particles averaged over all allowable configurations.

Substituting equations (I-14), (I-15), and (I-16) into equation (I-11), and noting equation (I-12),

$$\Xi = e^{PV/kT} = \sum_{N_1,\, N_2 \geq 0} Z_{N_1N_2} z_1^{N_1} z_2^{N_2} / N_1!N_2! \qquad \text{(I-17)}$$

Note that z_1 and z_2 are proportional to the absolute activities, λ_1 and λ_2. Since the fugacity is also proportional to λ, there must be a relation between z_2 and f_2. The fugacity has the property that $f \to P$ (P is the hydrostatic pressure) as $\rho \to 0$ (ρ is the density); or $f \to \rho kT$ as $\rho \to 0$. If $z \to \rho$ as $\rho \to 0$ (this will be shown later), then $z = f/kT$.

Taking the logarithm of both sides of equation (I-17) and expanding,

$$P/kT = z_1 + z_2 + b_{20}(T)z_1^2 + b_{11}(T)z_1z_2 + b_{02}(T)z_2^2 + \ldots \qquad \text{(I-18)}$$

where

$$b_{10} = b_{01} = 1 \qquad \text{(I-19)}$$

$$b_{11} = (Z_{11} - V^2)/V \qquad \text{(I-20)}$$

$$b_{20} = (Z_{20} - V^2)/2V \qquad \text{(I-21)}$$

$$b_{02} = (Z_{02} - V^2)/2V \qquad \text{(I-22)}$$

For the partial pressure of one component, equation (I-18) becomes

$$P_1/kT = x_1P/kT = z_1 + b_{20}z_1^2 + (1/2)b_{11}z_1z_2 + \ldots \qquad \text{(I-23)}$$

Substituting $z = f/kT$,

$$x_1P/kT = f_1/kT + b_{20}(f_1/kT)^2 + (1/2)b_{11}f_1f_2/(kT)^2 + \ldots \qquad \text{(I-24)}$$

The inverse of this equation is

$$f_1/kT = x_1P/kT + B_{20}(x_1P/kT)^2 + (1/2)B_{11}x_1x_2(P/kT)^2 + \ldots \qquad \text{(I-25)}$$

where

$$B_{20} = -b_{20} \tag{I-26}$$

$$B_{11} = -b_{11} \tag{I-27}$$

Equation (I-25) is the desired relation, and may be rearranged as[9]

$$f_1 = x_1 P[1 + B_{20}x_1(P/kT) + (1/2)B_{11}x_2(P/kT) + \ldots] \tag{I-28}$$

There are several points which require further explanation. It was previously assumed that $z \to \rho$ as $\rho \to 0$; this can be shown by considering that

$$\rho_i = z_i(\partial(P/kT)/\partial z_i)_{T,z_j,v} \tag{I-29}$$

Applying this to equation (I-23),

$$\rho_1 = z_1 + 2b_{20}z_1^2 + b_{11}z_1z_2 + \ldots \tag{I-30}$$

The inverse is

$$z_1 = \rho_1 - 2b_{20}\rho_1^2 - b_{11}\rho_1\rho_2 + \ldots \tag{I-31}$$

Thus, $z_1 \to \rho_1$ as $\rho_1 \to 0$.

Finally, some discussion should be given to the definition of B_{20} and B_{11}. From equations (I-23), (I-26), (I-27), and (I-31):

$$P_1/kT = \rho_1 + B_{20}(\rho_1)^2 + (1/2)B_{11}(\rho_1\rho_2) + \ldots \quad \text{(I-32)}$$

Equation (I-32) is just the virial expansion for one component of a binary mixture with virial coefficients B_{20} and B_{11}. Furthermore, from equations(I-20), (I-21), (I-26), and (I-27),

$$B_{11} = -(Z_{11} - V^2)/V \quad \text{(I-33)}$$

$$B_{20} = -(Z_{20} - V^2)/2V \quad \text{(I-34)}$$

The $Z_{N_1N_2}$, defined by equation (I-16), are configuration integrals given by

$$Z_{N_1N_2} = \int_V e^{-U_{N_1N_2}/kT} d\{N_1\}d\{N_2\} \quad \text{(I-35)}$$

where $d\{N_1\} = dr_1dr_2\ldots dr_{N_1}$ and $U_{N_1N_2}$ is a function which describes the potential interaction energy between N_1 and N_2 particles. Then

$$B_{20} = -1/2 \int_0^\infty (e^{-U_{20}/kT} - 1)4\pi r^2 dr \quad \text{(I-36)}$$

$$B_{11} = -\int_0^\infty (e^{-U_{11}/kT} - 1)4\pi r^2 dr \quad \text{(I-37)}$$

where U_{20} is the potential energy function for two molecules of component 1, and U_{11} is the function for one molecule of component 1 and one molecule of component 2.

Relation between Solute Interactions and the Activity Coefficient

In the phase equilibrium data which will be analyzed, the liquid phase consists mostly of one component, the solvent, held at constant temperature and pressure, and containing small numbers of molecules of the second component, the solute. The canonical ensemble for a mixture $Q(N_1, N_2, V, T)$ may be summed over the volume to obtain the isobaric partition function $\Delta^*_{N_2}$:

$$\Delta_{N_2} = \sum_V Q_V(N_1, N_2, T)e^{-PV/kT} \qquad \text{(I-38)}$$

In the actual experiment (dissolving a gas in a liquid), N_2 is not a fixed quantity. The function Δ_{N_2} is then summed over the distributions of the solute molecules:

$$\Gamma(N_1, P, T, \mu_2) = \sum_{N_2 \geq 0} \Delta_{N_2}(N_1, P, T)e^{N_2\mu_2/kT} \qquad \text{(I-39)}$$

Γ is a semi-grand partition function, open with respect to component two but closed with respect to component one, for a collection of systems held at a fixed temperature and pressure. The relation to thermodynamics is

$$\Gamma(N_1, P, T, \mu_2) = e^{-N_1\mu_1/kT} \qquad \text{(I-40)}$$

---

*The relations in this section are from Hill.[8,10] For simplicity, his notation is used here.

The quantity on the right in equation (I-39) is actually a power series in the absolute activity λ_2, since

$$\lambda_2 = e^{\mu_2/kT} \tag{I-41}$$

This quantity will be replaced by a more practical activity, a_2, with the properties $a_2 \to m_2$ as $m_2 \to 0$, where $m_2 = N_2/N_1$.

It will also prove advantageous later if equation (I-39) is put in a particular form. Dividing through by the leading term Δ_0, and making the substitutions (compare with equations (I-16) and (I-15))

$$X_N = N!\Delta_N\Delta_0^{N-1}N_1^N/\Delta_1^N \tag{I-42}$$

$$a_2 = \lambda_2(\Delta_1/\Delta_0 N_1) \tag{I-43}$$

where the subscript on N_2 has been dropped, since the sums are always over N_2. Then,

$$\Gamma/\Delta_0 = 1 + \sum_{N \geq 1} (X_N/N!)a_2^N \tag{I-44}$$

Referring again to equation (I-40), in the limit as $m_2 \to 0$,

$$N_1\mu_1(P, T, 0) = -kT\ln\Delta_0 \tag{I-45}$$

where $\mu_1(P, T, 0)$ is the chemical potential of the pure solvent.

Then defining

$$\mu_1'(P, T, a_2) = \mu_1(P, T, a_2) - \mu_1(P, T, 0) \qquad \text{(I-46)}$$

and noting from equation (I-40) that

$$-\mu_1(P, T, a_2)/kT = \ln\Gamma/N_1 \qquad \text{(I-47)}$$

then from (I-45), (I-46), and (I-47)

$$-\mu_1'(P, T, a_2)/kT = (1/N_1)\ln(\Gamma/\Delta_0) \qquad \text{(I-48)}$$

If either side of equation (I-48) is expressed as a power series in the activity a_2, then

$$-\mu_1'(P, T, a_2)/kT = (1/N_1)\ln(\Gamma/\Delta_0) = \sum_{j \geq 1} \theta_j(P, T)a_2^j \qquad \text{(I-49)}$$

The coefficients θ_j may be evaluated in terms of the integrals X_N by noting that

$$\Gamma/\Delta_0 = 1 + \sum_{N \geq 1} [\ln(\Gamma/\Delta_0)]^N / N! \qquad \text{(I-50)}$$

Then by substituting equation (I-49) on the right hand side and equation (I-44) on the left hand side of equation (I-50) and equating like coefficients, the following relations are found:

$$1!N_1\theta_1 = X_1 \tag{I-51}$$

$$2!N_1\theta_2 = X_2 - X_1^2 \tag{I-52}$$

$$3!N_1\theta_3 = X_3 - 3X_1X_2 + 2X_1^3 \tag{I-53}$$

Equation (I-42) gives the result that $X_1 = N_1$, so from equation (I-51), $\theta_1 = 1$.

The quantity m_2 is easily obtained from experimental data whereas a_2 is not. The relation between these can be found from the Gibbs-Duhem equation:

$$a_2[\partial(-\mu_1'/kT)/\partial a_2]_{P,T} = m_2 \tag{I-54}$$

Applying this to equation (I-49),

$$m_2(P, T, a_2) = \sum_{j \geq 1} j\theta_j(P, T)a_2^j \tag{I-55}$$

Assume there is an inverse to this series of the form

$$\ln\gamma_2' = -\sum_{k \geq 1} \delta_k(P, T)m_2^k \tag{I-56}$$

(the logarithm form is for later convenience). Then, since $m_2\gamma_2' = a_2$,

$$\ln a_2 = \ln\gamma_2' + \ln m_2 \tag{I-57}$$

Substituting equations (I-55) and (I-56) into equation (I-57),

$$\ln a_2 = \sum_{k \geq 1} -\delta_k(P, T) m_2^k + \ln\left[\sum_{j \geq 1} j\theta_j(P,T) a_2^j \right] \qquad \text{(I-58)}$$

Or

$$\ln a_2 = \sum_{k \geq 1} -\delta_k(P,T) \left[\sum_{j \geq 1} j\theta_j a_2^j \right]^k + \ln a_2 + \ln\left(1 + \sum_{j \geq 2} j\theta_j a_2^{j-1}\right) \qquad \text{(I-59)}$$

Then upon expanding the logarithm on the far right and equating like powers of a_2,

$$\delta_1 = 2\theta_2 \qquad \text{(I-60)}$$

$$\delta_2 = 3\theta_3 - 6\theta_2^2 \qquad \text{(I-61)}$$

Referring back to equation (I-56), it can be seen that the activity coefficient γ_2' has now been expressed as a power series in the molality m_2, with coefficients that can be related to configuration integrals (note equations (I-51)-(I-53)).

The task of evaluating the X_N begins with the assumption that solute-solute interactions can be characterized by virial coefficients B_N^* of the type used in the last section; for example, equation (I-36) would be analogous to B_2^*, with U_{20} describing the potential of average force between two solute molecules.

Actually, the exact relations would be found from an analysis

similar to that of the last section, but for a pure, single component gas. For such a situation, equations (I-16) and (I-17) become

$$Z_N(V, T)/N! = Q_N(V, T)V^N/Q_1^N(V, T) \tag{I-62}$$

and

$$e^{PV/kT} = \sum_{N \geq 0} Z_N(V, T)z^N/N! = 1 + \sum_{N \geq 1} Z_N(V, T)z^N/N! \tag{I-63}$$

Equation (I-18) reduces to

$$P/kT = \sum_{j \geq 1} b_j(T)z^j \tag{I-64}$$

By taking the logarithm of equation (I-63), expanding, and comparing the coefficients with those of equation (I-64),

$$b_1 = Z_1/1!V \tag{I-65}$$

$$b_2 = (Z_2 - Z_1^2)/2!V \tag{I-66}$$

From equation (I-62), $Z_1 = V$, therefore $b_1 = 1$ (recall $b_{10} = 1$). Substituting $-b_2 = B_2$, solving for the configuration integrals Z_N, and using the notation that will characterize solute interactions,

$$Z_1^* = V \tag{I-67}$$

$$Z_2^* = -2VB_2^* + V^2 \tag{I-68}$$

Thus, the solute-solute interactions are defined exactly as are the molecular interactions in a gas.

The second step in evaluating the X_N is to consider the nature of the solvent. Hill gives as an example an inert, incompressible liquid whose volume is just

$$V_0 = N_1 V_1 \tag{I-69}$$

An inert solvent is one whose molar volume does not change upon the addition of solute.

The solution is also incompressible, with the volume

$$V = V_0 + N_2 V_2 \tag{I-70}$$

for the pure solvent,

$$Q(N_1, N_2 = 0, V) = Q_0 \delta'(V - V_0) \tag{I-71}$$

where $\delta'(V - V_0)$ is the Dirac δ-function which may be used because of the assumption of incompressibility. Equation (I-71) means that pure solvent exists as only one state, that with $V = V_0$. In general, Q has only one value for each value of N_2, and

$$Q(N_1, N, V) = Q_0\delta'[V - (V_0 + NV_2)]Z_N^*(V) / N!\Lambda_2^{3N} \qquad (I\text{-}72)$$

where $Z_N^*/N!\Lambda_2^{3N}$ is the canonical ensemble partition function of the solute molecules (this could also be denoted as Q_{01}^{*N}). Then from equation (I-38)

$$\Delta_N = [e^{-P(V_0 + NV_2)/kT}]Q_0Z_N^*(V_0 + NV_2) / N!\Lambda_2^{3N} \qquad (I\text{-}73)$$

The desired result is near, since the X_N are defined in terms of the Δ_N. From equation (I-42)

$$X_2 = 2!\Delta_2\Delta_0N_1^2 / \Delta_1^2 \qquad (I\text{-}74)$$

Substituting equation (I-73) into equation (I-74) yields

$$X_2 = N_1^2 - 2N_1^2B_2^*/V_0 + 2V_2N_1^2/V_0 \qquad (I\text{-}75)$$

Then from equations (I-69), (I-52), and (I-60),

$$\delta_1 = -2[(B_2^*/V_1) - (V_2/V_1)] \qquad (I\text{-}76)$$

and from equation (I-56),

$$\ln\gamma_2'(P, T, m_2) = -2[(V_2/V_1) - (B_2^*/V_1)]m_2 \qquad (I\text{-}77)$$

Equation (I-77) gives the activity coefficient in terms of V_2, V_1, and B_2^*. V_2 will be the subject of the next section, V_1 is known from published data on the molar volume of pure solvent, and B_2^* will be left as the only unknown in the final equation.

The Scaled Particle Theory

There has been much work recently on a theory of solutions known as the scaled particle theory, which will be used here to provide theoretical values of the partial molar volume of the solute. The general approach presented here has mostly been taken from Pierotti.[11]

The chemical potential of a solute in some liquid solvent can be expressed as[12]

$$\mu_2^L = -\bar{U}_2 + P\bar{V}_2 + RT\ln(\Lambda_2^3/j_2) + RT\ln(N_2/V) \qquad \text{(I-78)}$$

where $\bar{U}_2$ is the potential energy of the solute in solution relative to infinite separation, P is the hydrostatic pressure, $\bar{V}_2$ is the partial molar volume of the solute, N_2/V is the number density of solute molecules in solution, and V/Λ_2^3 and j_2 are molecular partition functions.

Since

$$(\partial\mu_2/\partial P)_{T,N} = \bar{V}_2 \qquad \text{(I-79)}$$

then

$$\bar{V}_2 = -(\partial\bar{U}_2/\partial P) + [\partial(P\bar{V}_2/\partial P] + RT[\partial\ln(N_2/V)/\partial P] \qquad \text{(I-80)}$$

The last term of this equation can be put in a more convenient form. Since for sufficiently dilute solutions $V = N_1\bar{V}_1$, then

$$(N_2/V) = (N_2/N_1\bar{V}_1) = (X_2/\bar{V}_1) \qquad \text{(I-81)}$$

The evaluation of the other terms is more difficult; this is where the scaled particle theory is used. Consider the solution process to occur in two steps:

(1) A cavity, just large enough to accommodate the solute molecule, is created in the solvent. The reversible work required to create a mole of such cavities is $\bar{G}_c$.

(2) The solute molecule is introduced into the cavity. The molecule interacts with the solvent according to some potential function, yielding a reversible work of interaction, $\bar{G}_i$.

The sum of these terms, $\bar{G}_i + \bar{G}_c$, may be identified with $-\bar{U}_2 + P\bar{V}_2$ of equation (I-78). Making this substitution along with (I-81) yields

$$V_2 = (\partial\bar{G}_c/\partial P)_{T,N} + (\partial\bar{G}_i/\partial P)_{T,N} + RT\beta_T \qquad \text{(I-82)}$$

where β_T is the isothermal compressibility of the solvent.

Reiss, Frisch, Helfand, and Lebowitz[13] have developed an expression for the free energy of cavity formation. They first approximated $\bar{G}_c$ as

$$\bar{G}_c = K_0 + K_1 r + K_2 r^2 + K_3 r^3 \qquad \text{(I-83)}$$

where r is the cavity radius given by $(\sigma_1 + \sigma_2)/2$ and σ is defined as the distance of closest approach of two molecules originally infinitely far apart with no kinetic energy.

These authors evaluated the coefficients and found

$$K_0 = RT\{-\ln(1 - y) + 9/2[y/(1 - y)]^2\} - (\pi P\sigma_1^3/6) \qquad \text{(I-84)}$$

$$K_1 = -(RT/\sigma_1)\{6y/(1 - y) + 18[y/(1 - y)]^2\} + \pi P\sigma_1^2 \qquad \text{(I-85)}$$

$$K_2 = (RT/\sigma_1^2)\{12y/(1 - y) + 18[y/(1 - y)]^2\} - 2\pi P\sigma_1 \qquad \text{(I-86)}$$

$$K_3 = (4/3)\pi P \qquad \text{(I-87)}$$

where $y = \pi\rho_1\sigma_1^3/6$ is the reduced number density of the solvent, and the other symbols have their usual meaning.

Substituting the relations (I-84)-(I-87) in equation (I-83) yields, after some rearranging,

$$\bar{G}_c/RT = -\ln(1 - y) + 3yR/(1 - y) + [3y/(1 - y) + (9/2)y/(1 - y)^2]R^2 + N_0yPR^3/\rho_1RT \qquad \text{(I-88)}$$

where $R = \sigma_2/\sigma_1$. Then

$$(\partial\bar{G}_c/\partial P)_{T,N} = y\beta_T RT(1 - y)^{-3}[(1 - y)^2 + 3R(1 - y + R(1 + 2y))] + N_0\pi\sigma_2^3/6 \qquad \text{(I-89)}$$

The interaction energy E_i may be found by summing all of the individual solute-solvent interactions averaged over all configurations of the solvent. This sum can be replaced by the integral

$$\bar{E}_i = N_0 \int_V \xi_i(r) 4\pi r^2 \rho_1 g(r) dr \qquad \text{(I-90)}$$

where $\xi_i(r)$ is the function that describes pairwise interactions, ρ is the solvent number density, and $g(r)$ is the radial distribution function. Since $g(r)$ is generally unknown, it may be approximated as being unity outside the cavity radius. Then if the Lennard-Jones (6-12) potential describes $\xi_i(r)$,

$$\bar{E}_i = N_0 \int_{\sigma_{12}}^{\infty} 4\varepsilon_{12}[(\sigma_{12}/r)^6 - (\sigma_{12}/r)^{12}] \rho 4\pi r^2 dr \qquad \text{(I-91)}$$

This is easily solved, and is

$$\bar{E}_i = -(32/9) N_0 \pi \rho_1 \sigma_{12}^3 \varepsilon_{12} \qquad \text{(I-92)}$$

It is known from thermodynamics that $G = E + PV - TS$. It might be assumed that the volume of the cavity created in step one of the solution process might decrease somewhat during step two. Since a decrease in volume would probably change the solvent configuration about the cavity, the "PV" and "TS" terms should be considered. However, there is no known procedure for calculating these changes. Knowing that these terms should be small, the approximation will be made that $\bar{G}_i = \bar{E}_i$.

Then substituting this in equation (I-92), and taking the pressure derivative,

$$(\partial \bar{G}_i/\partial P)_{T,N} = (-32/9)N_0\pi\sigma_{12}^3\epsilon_{12}[-(N_0/V_1^2)(\partial V_1/\partial P)] = \beta_T \bar{G}_i \qquad \text{(I-93)}$$

Thus, $\bar{V}_2$ may be found by substituting equations (I-93) and (I-89) in equation (I-82). Since the calculations involved here have assumed the presence of only one solute molecule in the solvent volume, then the $\bar{V}_2$ calculated here is in fact $\bar{V}_2^{\infty}$.

Summary

The relation between the activity coefficient in equation (I-8) and that in equation (I-77) is

$$\gamma_2 = \gamma_2'(1 + m_2) \qquad \text{(I-94)}$$

Substituting equations (I-94) and (I-77) into equation (I-8) yields

$$\partial \ln(f_2/x_2)/\partial P = \partial[-2\{(V_2/V_1) - (B_2^*/V_1)\}m_2]/\partial P + (\partial m_2/\partial P)/(1 + m_2) + \bar{V}_2^{\infty}/RT \qquad \text{(I-95)}$$

This equation may be further simplified by noting that under the conditions of infinite dilution, $1/(1 + m_2) = 1$, and $V_2 = V_2^{\infty}$. Then by neglecting the compressibility and expressing all volumes as molar volumes,

$$B_2^* = (1/2)\bar{V}_1[\partial \ln(f_2/x_2)/\partial P - (\bar{V}_2^\infty/RT)]/(\partial m_2/\partial P) + \bar{V}_2^\infty - \bar{V}_1/2 \qquad \text{(I-96)}$$

The right side of equation (I-96) can be evaluated from experimental data and the equations presented in this chapter.

CHAPTER III

EXPERIMENTAL DATA

The methods developed in the previous section were applied to phase equilibrium data on the He-Ar, [1,2] Ne-Ar,[3] and H_2-Ar[4] systems. Generally, the experimental procedure employed in these studies was to inject some of the solute gas into a closed vessel containing some condensed argon held at a fixed temperature. Some solute gas would dissolve in the argon; mechanical agitation would insure that equilibrium was reached. Then samples of the liquid and vapor phases were taken for gas chromatographic analysis; the temperature and total hydrostatic pressure were measured at the same time. The GC analysis provides the liquid and vapor compositions, which are then known as a function of temperature and pressure.

Volk and Halsey[4] used a volumetric apparatus such that measured numbers of moles of hydrogen and argon could be mixed in a cell of known volume. From measurements of the temperature and pressure of the gas mixture in the cell, the liquid and vapor compositions were calculated.

The solubility of these gases in argon is not very high, so that the theoretical procedure of summing over the distributions of small numbers of solute molecules in systems held at fixed temperature, pressure, and number of solvent molecules is appropriate.

The data may be characterized as follows. The liquid phase composition of the He-Ar system was reported by Sinor and Kurata[2] for four

temperatures from 93° to 148°K, and for pressures up to 136 atm. The smoothed data of Mullins and Ziegler[1] gave the liquid and vapor phase composition at 5° intervals from 85° to 110°K, and at 5 atm. intervals up to 120 atm. Volk and Halsey[4] provide the same data for the H_2-Ar system for seven temperatures between 87° and 140°K, and for pressures up to 100 atm. Finally, Streett[3] provides the liquid and vapor composition of the Ne-Ar system for seven temperatures between 84.42° and 129.93°K, and for pressures to ∿70 atm.

CHAPTER IV

RESULTS

The first step in the application of equation (I-96) is to calculate the fugacity according to equation (I-28).* Hirschfelder, Curtis and Bird[14] provide a convenient means for calculating the required virial coefficients from the Lennard-Jones interaction parameters. First, the reduced temperature is defined as

$$T^{\dagger} = kT/\varepsilon \qquad \text{(I-97)}$$

From $T^{\dagger}$ and table 1-B, $B^{\dagger}$ is found, which is defined as

$$B^{\dagger} = B/b_0 \qquad \text{(I-98)}$$

where B is the required second virial coefficient and $b_0 = (2/3)\pi N_0\sigma^3$. This procedure is followed even if a mixed virial coefficient is needed; but then,

---

*Sinor and Kurata[2] did not report the gas phase composition, which is required in this equation. The He pressure was taken to be the total pressure less the vapor pressure of Ar, which was calculated according to $P_{Ar} = P_0\exp[\bar{V}_1(P - P_0)/RT]$ where P is the total pressure and P_0 is the vapor pressure of pure Ar. Then $X_2 = P_{(He)}/P$.

$$b_{0(12)} = (1/8)\{b_{0(1)}^{1/3} + b_{0(2)}^{1/3}\}^3 \qquad \text{(I-99)}$$

$$\varepsilon_{(12)}/k = (\varepsilon_1/k)^{1/2}(\varepsilon_2/k)^{1/2} \qquad \text{(I-100)}$$

The mixed coefficient calculated in this manner is equal to half of B_{11} (note the relation between equations (I-36) and (I-37)). Table 1 gives the values of the Lennard-Jones interaction parameters used in these calculations.

Next, the derivatives required in equation (I-96) were found by plotting $\ln(f_2/x_2)$ and m_2 (= x_2/x_1) versus P_{Total}, and then fitting by a least squares analysis those points which were judged to lie on the initial straight line (sometimes the lowest pressure measurement was discarded, owing to a larger relative experimental error in this pressure region). Examples of such plots are shown in figures 1 and 2.

The scaled particle theory was used to calculate $\bar{V}_2^{\infty}$ according to equations (I-93), (I-89), and (I-82). This calculation required, besides the parameters given in table 1, the molar volume and isothermal compressibility of Ar. Mullins and Ziegler[1] give the coefficients and the vapor pressure P_0 of the following equation for Ar at 5° intervals from 85° to 145°K (see appendix A):

$$\bar{V}_1 = A_1 + A_2(P - P_0) + A_3(P - P_0)^2 \qquad \text{(I-101)}$$

The isothermal compressibility, $\beta_T = -(1/V)(\partial V/\partial P)_T$, is then just $-A_2/A_1$. Table 2 shows the values of $\bar{V}_2^{\infty}$ calculated by this method, and

Table 1. The Values of the Lennard-Jones Interaction Parameters Used in this Study

Gas	ε/k (°K)	σ (Å)
He	10.8	2.57
Ne	33.7	2.76
H_2	36.7	2.96
Ar	125.2	3.40

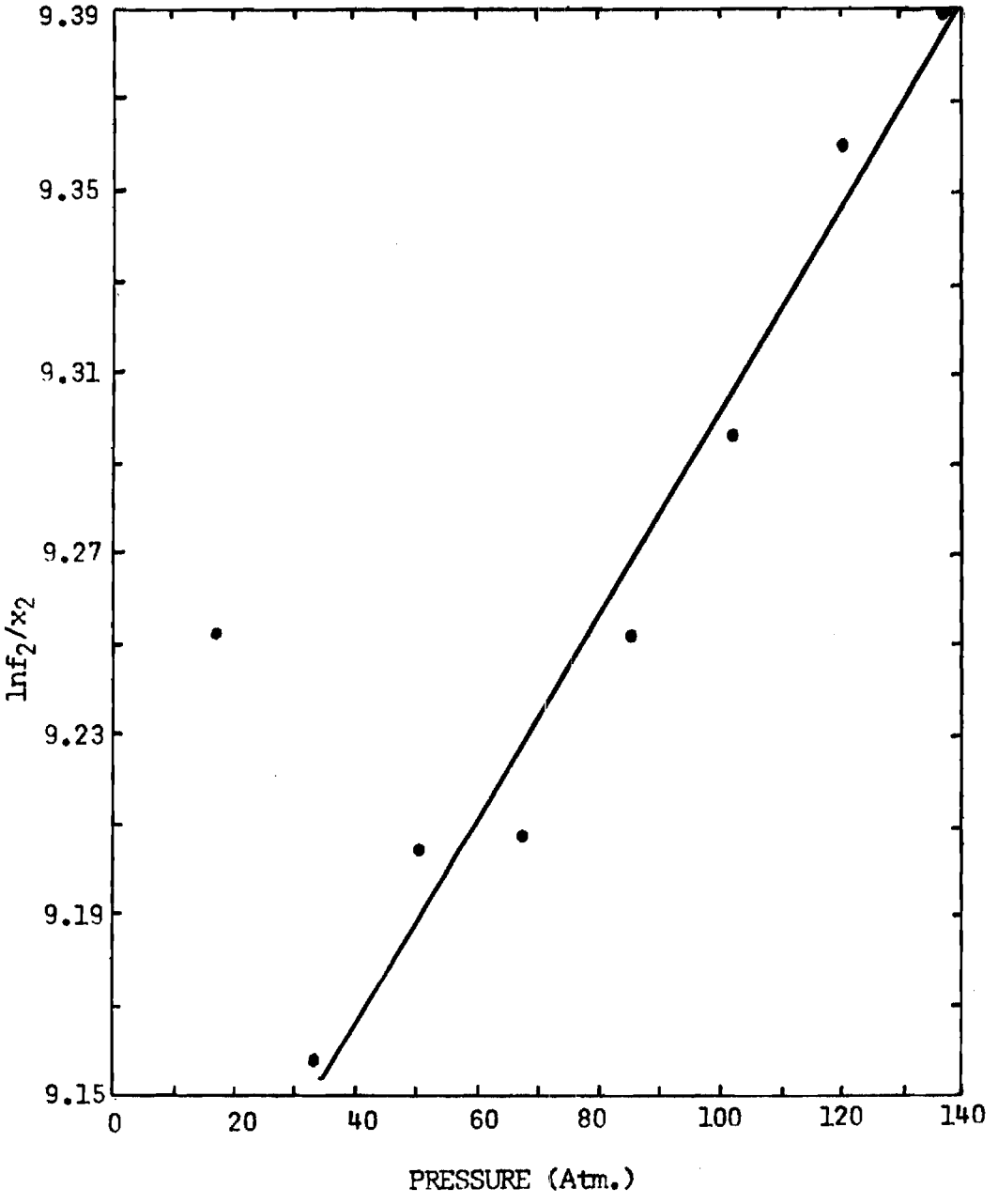

Figure 1. A Plot of $\ln f_2/x_2$ versus Pressure (from Sinor and Kurata's data at 93.2° K)

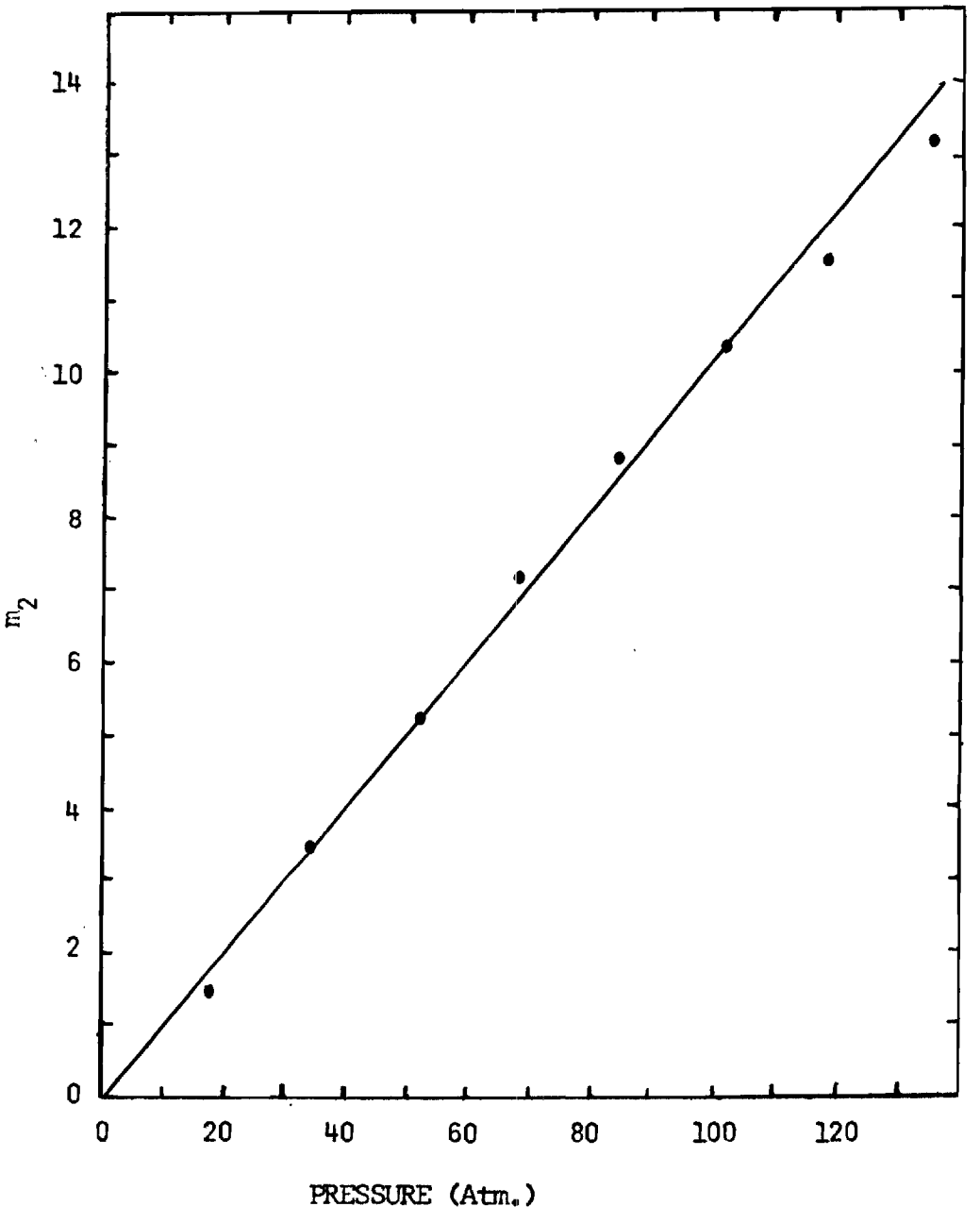

Figure 2. A Plot of m_2 vs. Pressure (from Sinor and Kurata's Data at 93.2°K)

Table 2. Values of $\bar{V}_2^{\infty\dagger}$ for Several Solutes in Liquid Argon

Scaled Particle Theory						Volk and Halsey	
He		Ne		H_2		H_2	
T	$\bar{V}_2^{\infty}$	T	$\bar{V}_2^{\infty}$	T	$\bar{V}_2^{\infty}$	T	$\bar{V}_2^{\infty *}$
85	23.8	84.42	23.4	87.0	28.4	87.0	30
90	28.5	87.42	26.0	94.2	33.3	94.2	30
95	32.6	95.82	32.5	100.0	37.6	100.0	31
100	36.2	101.94	36.0	110.0	43.0	110.0	34
105	39.1	110.78	40.0	120.0	45.3	120.0	36
110	41.5	121.36	42.5	130.0	49.7	130.0	39
93.2#	31.2	129.93	43.2	140.0	50.1	140.0	44
113.2	42.9						
133.2	44.8						
148.2	40.5						

† The values are given in cm^3/mole; the temperatures are in °K.

* Estimated uncertainty is ±4 cm^3/mole; values were measured at H_2 concentrations of 2-5 mole percent, and pressures under 60 atm.

\# These last four values are for Sinor and Kurata's data.

also measured values of $\bar{V}_2^{\infty}$ for H_2 reported by Volk and Halsey.[4]

B_2^* can now be calculated according to equation (I-96). These values are given in table 3, and are presented graphically in figure 3.

Table 3. Values of $B_2^{*\dagger}$

He		Ne		H_2	
T	B_2^*	T	B_2^*	T	B_2^*
85	-171	84.42	-62.3	87.0	-12.2
90	-176	87.42	-46.5	94.2	-16.3
95	-186	95.82	-59.7	100.0	-18.2
100	-161	101.94	-48.3	110.0	-6.3
105	-126	110.78	-36.3	120.0	-6.3
110	-90	121.36	-31.9	130.0	-0.1
93.2	-239	129.93	-28.0	140.0	+7.03
113.2	-210				
133.2	-77				
148.2	-12				

† The values are given in cm^3/mole; the temperatures are in °K.

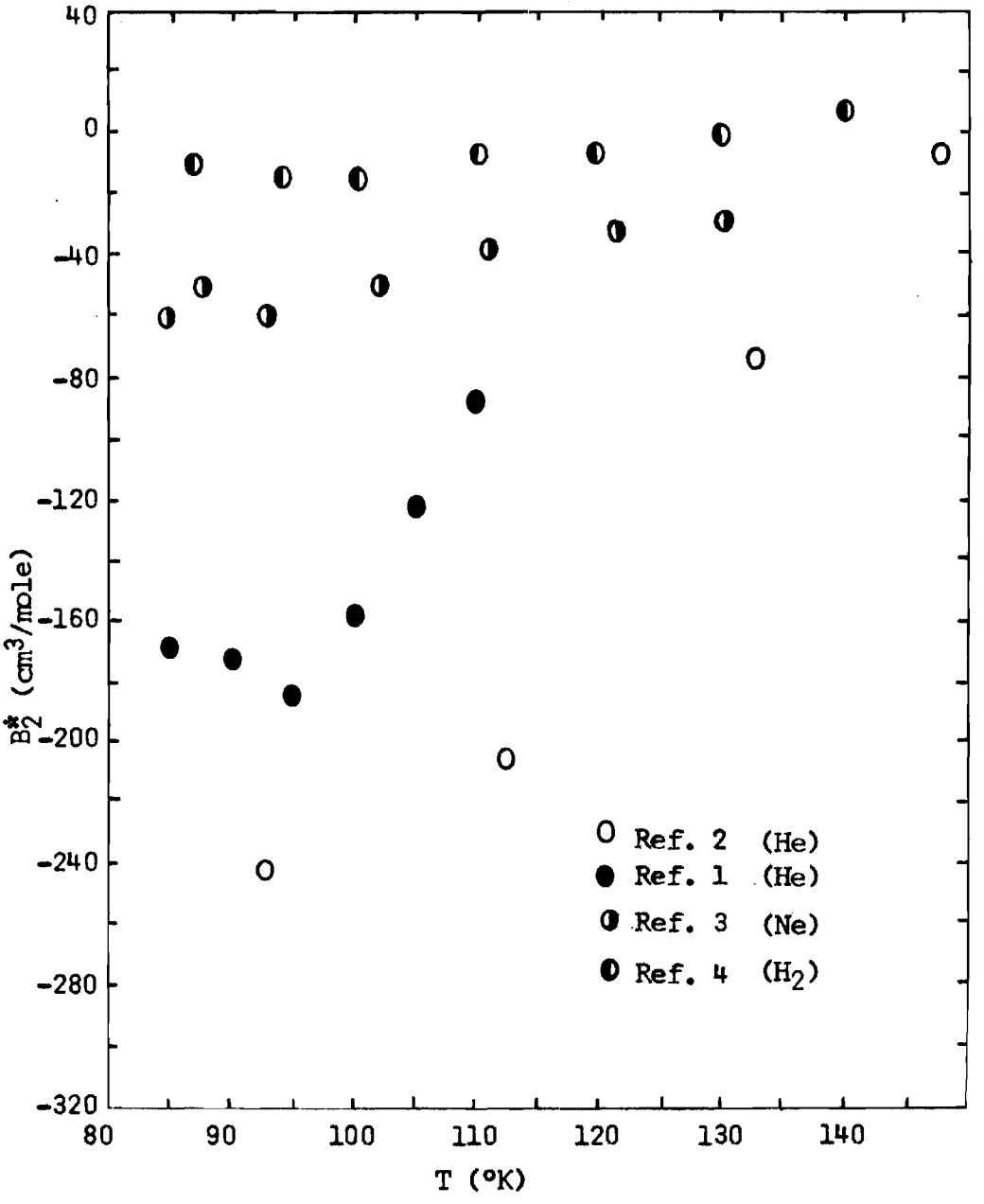

Figure 3. Experimental Values of B_2^* as a Function of the Temperature

CHAPTER V

DISCUSSION

Figure 4 presents the values of the second virial coefficients for He, Ne, and H_2 when these exist as dilute gases. A comparison between figures 3 and 4 shows a large difference in the values of these coefficients when the surrounding medium changes from a vacuum to a dense, interacting fluid. An examination of equation (I-36) shows that this change must result from a change in U_{20}, the potential of average force between the two molecules. Since it is unreasonable that this results from an increase in the dispersion interactions (actually, the dispersion interactions should decrease),[5] an alternative explanation must be found.

It must first be assumed that configurations of solute molecules are not independent of those of the solvent. This is equivalent to saying that the solute molecules are not dissolved in the void spaces of the liquid (hence movement is not restricted to motion through void channels); if this were not so, the partial molar volumes of the solutes would be negligibly small (also, recall that step one of the solution process of the scaled particle theory requires creation of a volume large enough to accommodate the solute molecule).

A different configuration of solute molecules must therefore result in a different configuration of the solvent. For the experimental systems which were analyzed, the partial molar volume of the solutes and

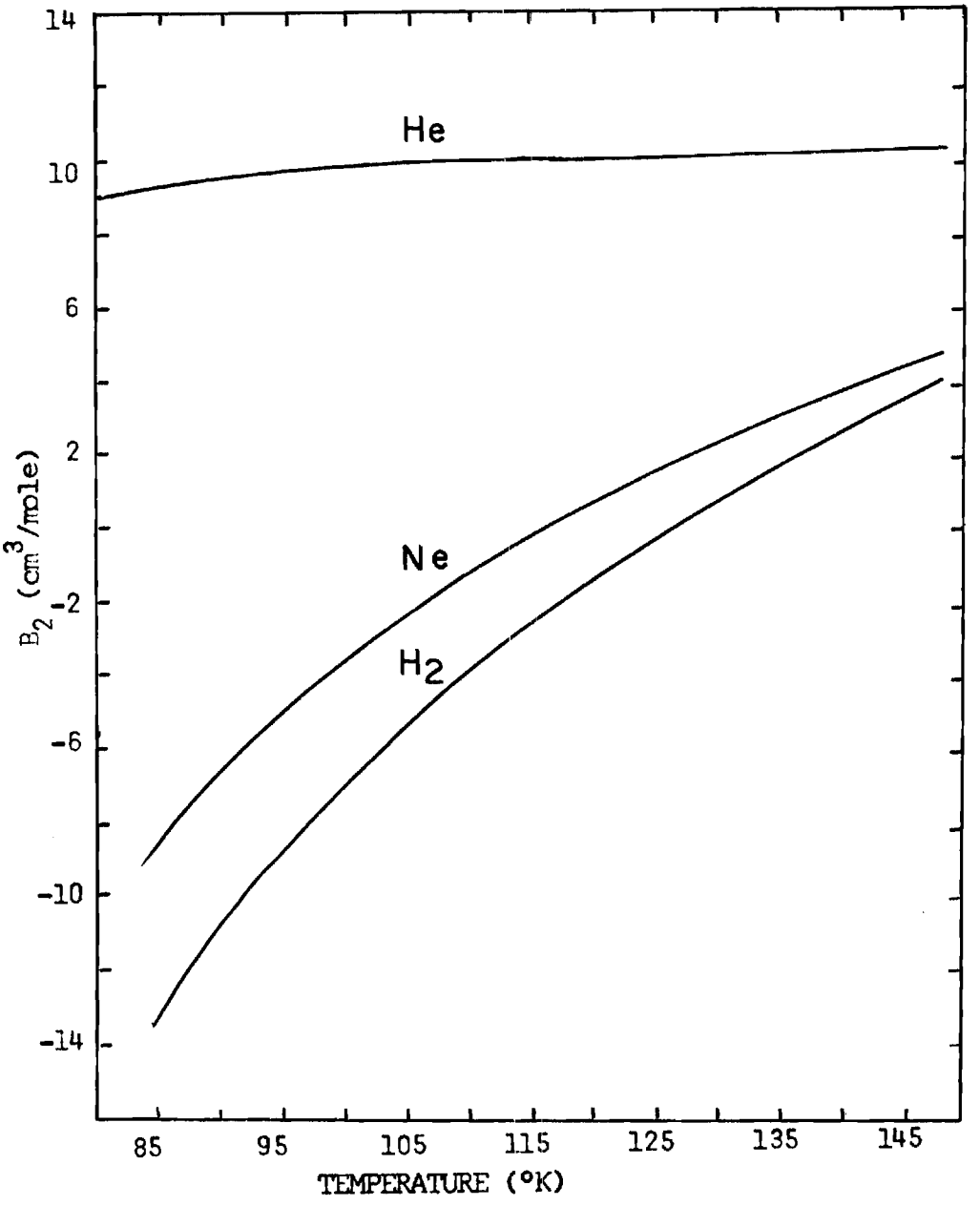

Figure 4. Values of Gas Phase Virial Coefficients for He, Ne, and H_2

the solvent were roughly equal; in such a situation, different solute configurations can be achieved in a rough manner by simply trading the positions of solute molecules with solvent molecules.

This notion can be used to calculate the potential energy of a solute as a function of its position in the solvent. Consider first the situation shown in figure 5, where solvent molecules are labelled as 1 and solute molecules as 2. The solute-solvent pair in the center of figure 5A will trade positions, resulting in the configuration shown in figure 5B. Denoting the interaction energy between molecules 1 and 2 located a distance "a" apart as $E_{12}(a)$, then the energies of the systems shown in figures 5A and 5B are

$$E_A = E_{11}(a - x) + E_{12}(a + x) + E_{11}(a + x) + E_{12}(a - x) + E_{12}(2x) + E_{11}(2a) \qquad \text{(I-102)}$$

$$E_B = E_{11}(a + x) + E_{12}(a - x) + E_{11}(a - x) + E_{12}(a + x) + E_{12}(2x) + E_{11}(2a) \qquad \text{(I-103)}$$

The difference in energy between the two configurations is

$$\Delta E = E_B - E_A = 0 \qquad \text{(I-104)}$$

Since all the molecules in the solvent may be represented as these fixed, symmetrical pairs, then the potential energy of the solute molecule is independent of position in the solvent (as long as it is

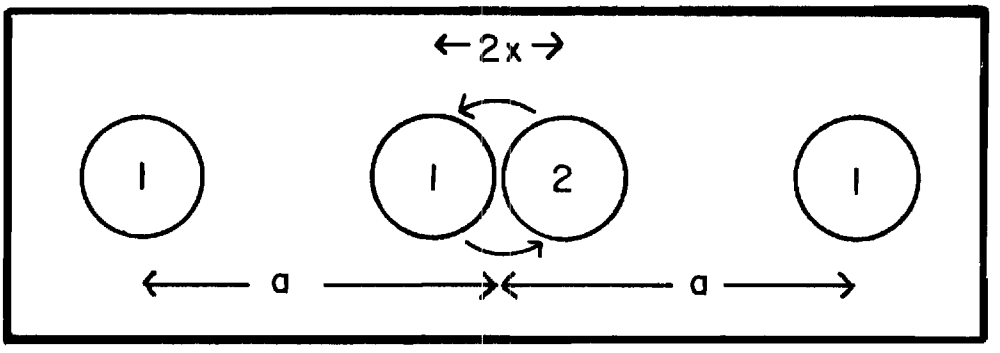

5A. The initial configuration, before the pair of molecules in the center have traded positions. The other two molecules are located symmetrically about the midpoint between the center pair.

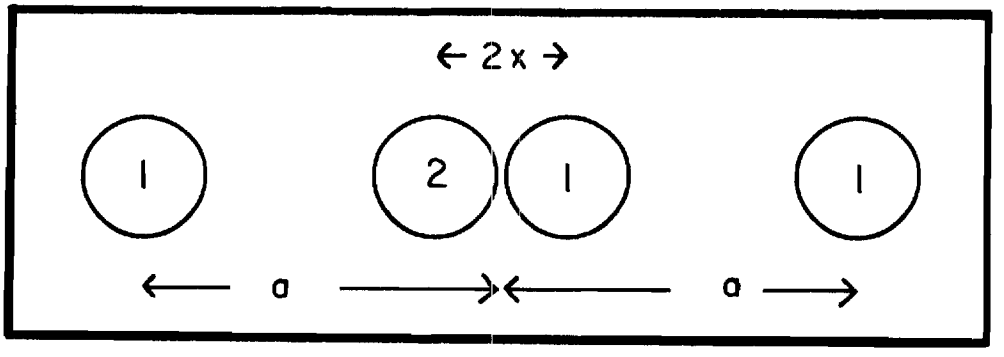

5B. The final configuration.

Figure 5. Configurations of One Solute Molecule in Otherwise Pure Solvent

not near the surface).

This situation changes if there is a second solute molecule in the vicinity. Then one of the fixed solvent molecules will find this second solute as its partner, and these do not represent a symmetrical pair. All other solvent molecules may be treated as symmetrical pairs as before, and need not be considered further. The situation is shown in figure 6, and, as before, the energy of the system shown in figure 6A is

$$E_A = E_{21}(a - x) + E_{22}(a + x) + E_{11}(a + x) + E_{21}(a - x) + E_{12}(2x) + E_{12}(2a) \qquad \text{(I-105)}$$

and

$$E_B = E_{21}(a + x) + E_{22}(a - x) + E_{11}(a - x) + E_{21}(a + x) + E_{12}(2x) + E_{12}(2a) \qquad \text{(I-106)}$$

Then

$$\Delta E = E_B - E_A = E_{22}(a - x) - E_{22}(a + x) + E_{11}(a - x) - E_{11}(a + x) + 2E_{12}(a + x) - 2E_{12}(a - x) \qquad \text{(I-107)}$$

This model shows that the configurations which result in closer solute-solute distances must also contain some closer solvent-solvent pairs, while some solvent-solute distances must increase. Thus, as the solute-

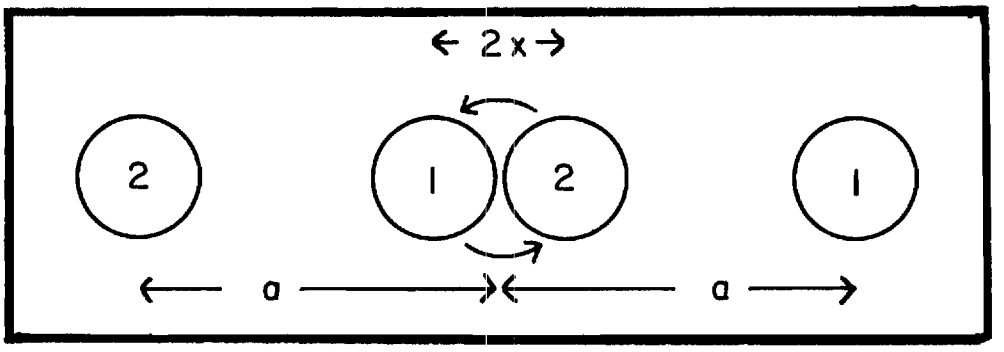

6A. The initial configuration as in 5A, but in the vicinity of a second solute molecule.

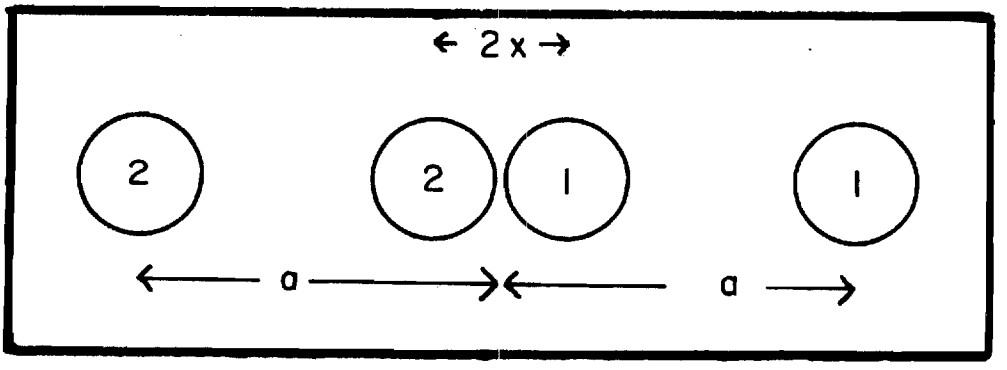

6B. The final Configuration, where the solute molecules are closer together.

Figure 6. Configurations of Two Solute Molecules in Otherwise Pure Solvent

solute dispersion interactions change, the solvent interactions must change accordingly, as in equation (I-107).

Assume that the Lennard-Jones (6-12) potential describes these pairwise dispersion interactions. Let r be the distance between solute molecules, and, in analogy with equation (I-107),

$$U^* = 4\varepsilon_1\sigma_1^6\,[(1/r)^6 - (\sigma_1^6/r^{12})] + 4\varepsilon_2\sigma_2^6[(1/r)^6 - (\sigma_2^6/r^{12})] - 8\varepsilon_{12}\sigma_{12}^6[(1/r)^6 - (\sigma_{12}^6/r^{12})] \qquad \text{(I-108)}$$

If the approximation is made that the repulsive terms are all equal to σ_1^6/r^{12}, then

$$U^* = 4\varepsilon^*[(\sigma_1/r)^6 - (\sigma_1/r)^{12}] \qquad \text{(I-109)}$$

where $\varepsilon^* = \varepsilon_1 + \varepsilon_2(\sigma_2/\sigma_1)^6 - 2\varepsilon_{12}(\sigma_{12}/\sigma_1)^6$. Table 4 contains values of ε^*/k, calculated from data in table 1. Then U^* from equation (I-109) may be substituted in equation (I-36) to find B_2^*. Alternatively, of course, the tables in Hirschfelder, Curtis, and Bird may again be used to perform this integration; the resulting values of B_2^* are given in figure 7, along with the past experimental results for comparison.

The model just presented is rather crude, but its very physical basis makes it attractive, and it does a fair job of predicting the experimental results. One of its obvious faults is that it does not depend on the density of the solvent. As the density decreases (the density of Ar decreases by a factor of two when the temperature

Table 4. Values of ϵ^*/k

Gas	ϵ^*/k (°K)
He	93.5
Ne	63.1
H_2	50.4

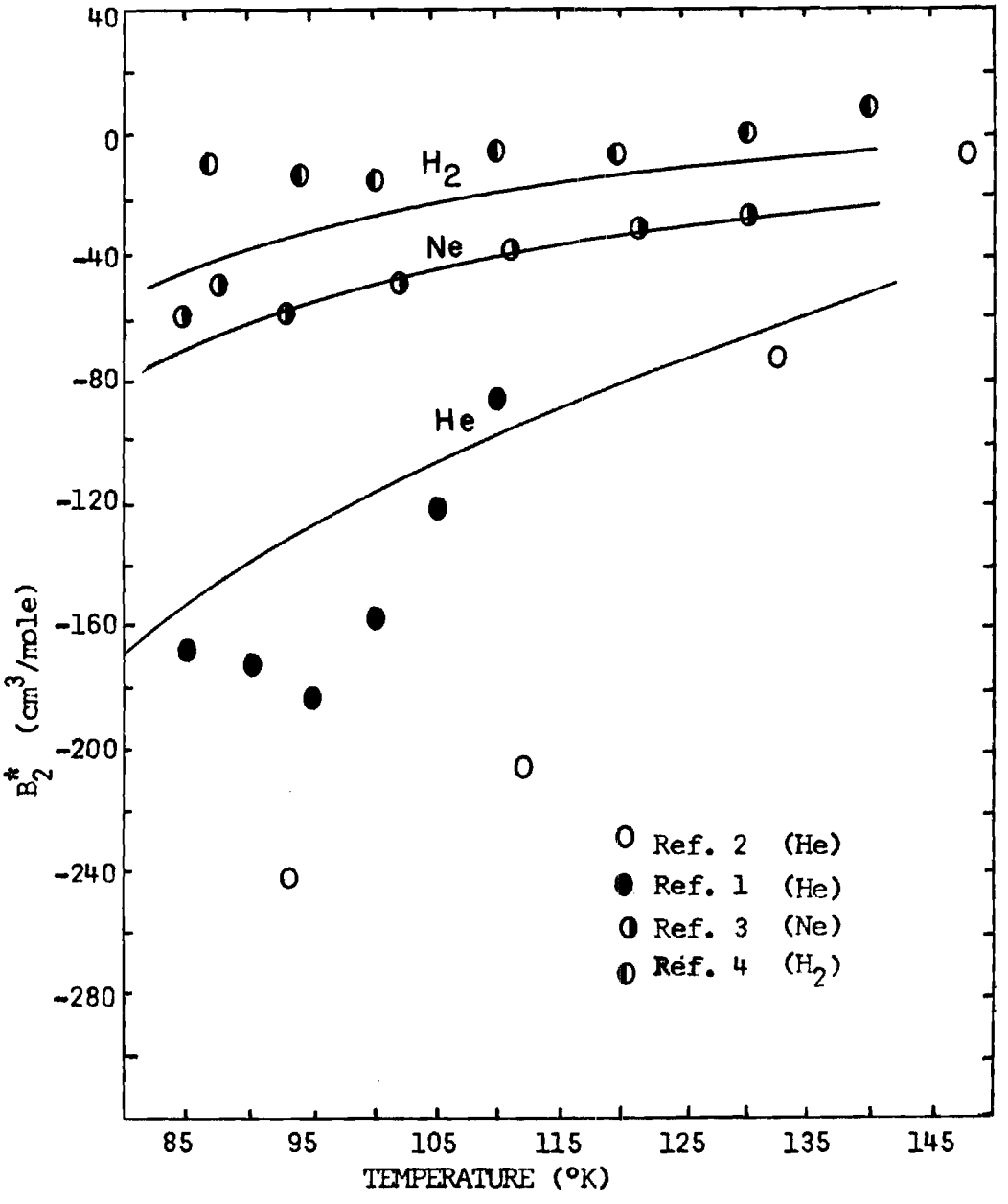

Figure 7. B_2^* as Calculated from Equation (1-109)

increases from 85° to 145°K), B_2^* must begin to approach the dilute gas values (the experimental results appear to do this). This would indicate that a density (or temperature) dependent potential function is required.

In the process of dissolving a molecule, solute-solvent interactions are created at the expense of solvent-solvent interactions. The difference in the energy between these types of interactions contributes to the work, W, required to dissolve the solute molecules. The change in energy when two solute molecules approach each other is also related to changes in such interactions, and might therefore be related to W, which would, of course, reflect such variables as solvent density.

The Henry's Law constant is defined as

$$K_H = \lim_{x_2 \to 0} f_2/x_2 \qquad \text{(I-110)}$$

It is therefore the value of f_2/x_2 at $P = P_0$, and may be found from a plot such as figure 1. Thus it is independent of any of the quantities used to find B_2^* in equation (I-96). Values of K_H are given in table 5. The Henry's Law constant is related to the work W required to dissolve the solute by[11]

$$W = RT\ln(K_H\bar{V}_1/RT) \qquad \text{(I-111)}$$

The quantity δW, where δ is an adjustable fraction, is now substituted for ε^* in equation (I-109). The value of δ is changed until a good fit

Table 5. Values of K_H, Determined from the Experimental Data

T(°K)	K_H (He-Ar)[1]	T(°K)	K_H (He-Ar)[2]	T(°K)	K_H (Ne-Ar)[3]	T(°K)	K_H (H_2-Ar)[4]
85	13700	93.2	8740	84.4	1130	87.0	845
90	10300	113.2	3370	87.4	1030	94.2	754
95	7870	133.2	1440	95.8	977	100.0	694
100	6100	148.2	489	101.9	860	110.0	600
105	4770			110.8	721	120.0	530
110	3760			121.4	571	130.0	456
				129.9	430	140.0	402

Note: References are to the source of data from which these numbers were determined.

to the experimental values of B_2^* is obtained. The results when $\delta = 0.40$ are shown in figure 8, along with the past experimental results for comparison.

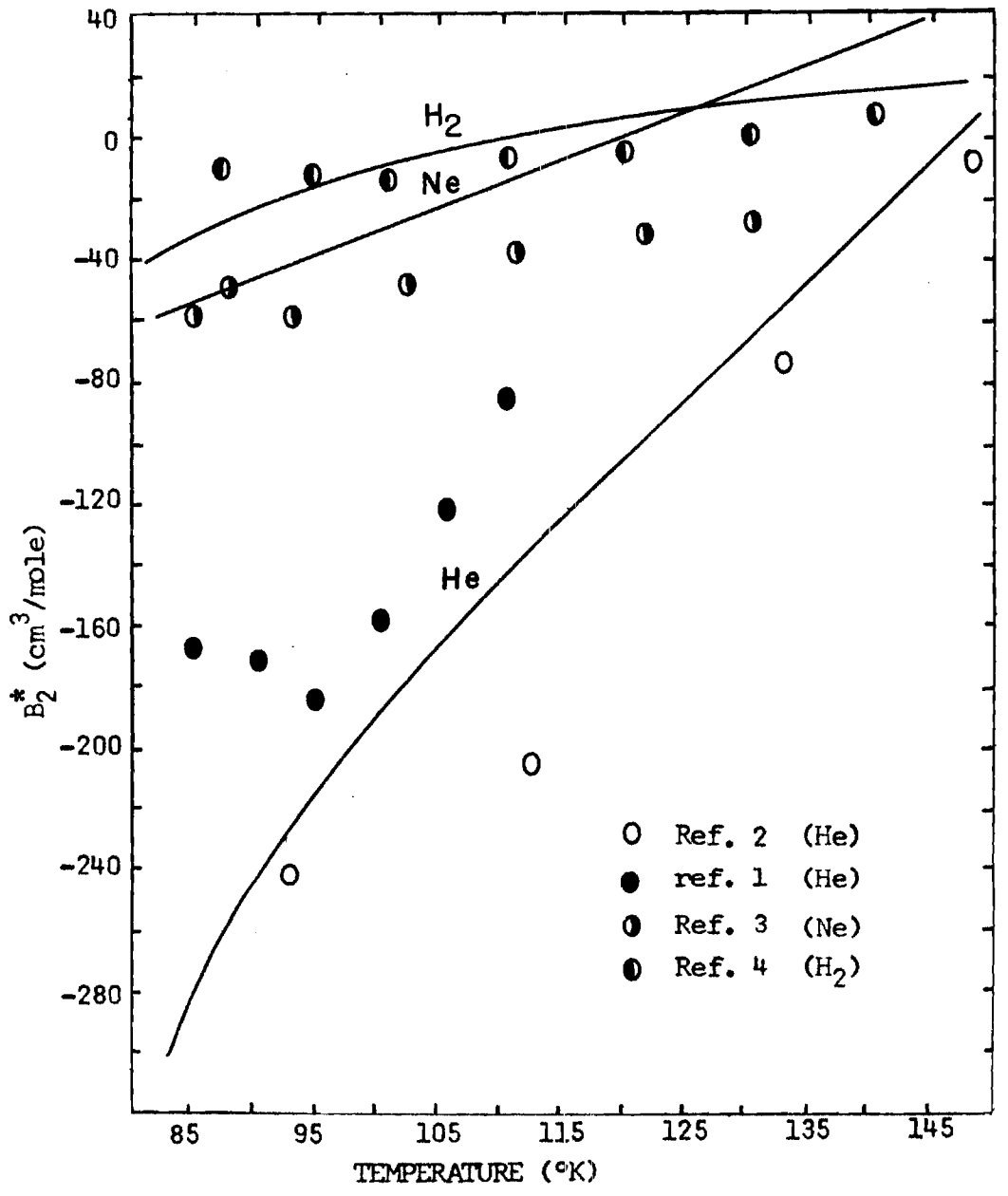

Figure 8. Values of B_2^* as Calculated from the Henry's Law Constant

CHAPTER VI

CONCLUSION

Assessment of Results

The results presented here (compare figures 3 and 4) show that the attractive forces between molecules in solution are different from the forces in the gas phase, but not in a manner that can be accounted for simply by assuming a reduction in the pair potential when in solution. Instead, a model which assumed that the solvent exerted some additional force was reasonably successful in predicting the experimental results. Values of effective force constants are given in table 4.

From the success of this model, it may be considered that the potential energy of both the solute and the solvent vary with solute-solute separation, and therefore both must be considered before solute-solute behavior can be determined. This would be particularly important in aqueous solutions, because of a rather large solvent-solvent interaction energy.

Recommendations for Future Work

This analysis should be extended to other systems, not only to provide a check on the conclusions drawn in this work, but also to increase the number of experimental values which can be compared with various theoretical treatments. The new systems should be of increasing differences in the interaction energies of the solute and the solvent.

The results of the present treatment partly rely on the results of the scaled particle theory. It would be advantageous to use experimental values of the partial molar volumes of the solutes, and future experiments should obtain these.

Future studies should look at aqueous solutions, not only because water is the most common and interesting reaction medium, but also because the interaction energy of the dipolar water molecules is so large.

Some of the commonly observed behavior of solutes in water is consistent with the conclusions just drawn. For example, it would be expected that two molecules composed of a hydrocarbon tail at one end and a polar group at the other end would interact with each other in aqueous solution as follows. The hydrocarbon tails interact relatively little with the water, and the solvent forces them together, whereas the polar ends may interact strongly with the water dipoles and would therefore be forced apart, in order to increase their interaction with the solvent. Such behavior is commonly observed for soap molecules and in micelle formation.

Conceivably, it would be possible to experimentally determine values of B_2^* in water for a partial series of several groups of molecules, such as hydrocarbons, alcohols, ketones, amines, etc., and determine the interactions between specific groups; for example, carbonyl groups. It might then be possible to determine the role of the solvent in such problems as enzyme-substrate bonding, for example. (It must be mentioned that the equations presented in this work are not directly applicable to aqueous solutions; this includes equation (I-96).)

Possibly some relation between pair interactions in solution and surface tension could be investigated. Surfactants tend to be concentrated near the liquid surface for probably much the same reason that solute molecules may be forced together. Imagine in figure 5A that the solute-solvent pair in the center are near the liquid surface, so that many solvent molecules in the liquid do not find a solvent molecule symmetrically located from the midpoint of the central pair. Each of these molecules would contribute a term analogous to equation (I-107) (less the E_{22} term and one E_{12} term), with the result that solvent-solvent interactions decrease and solute-solvent interactions increase as the solute moves into the bulk away from the surface. Salts, for example, do not raise the surface tension of water because they have a low concentration in the surface region. It might then be inferred, from the conclusions drawn in this work, that this is because the solute-solvent ion-dipole interaction is stronger than the solvent-solvent dipolar interaction. Ion pairs are then kept apart in water solutions because of this, and also because the charges on the ions may be masked by the water dipoles (reducing the E_{22} term in equation (I-107)).

PART TWO

THE INTERACTION BETWEEN KRYPTON AND THE (1, 1, 0) FACE OF COPPER SINGLE CRYSTALS

CHAPTER I

INTRODUCTION

Physical adsorption and imperfect gas behavior are two closely related phenomena associated with molecular interactions. The theory of non-ideal gas behavior is much more developed, and has often been applied to physical adsorption problems. The theoretical treatment used in this work is an example of this, and the parallels between physical adsorption and the better understood phenomena of imperfect gas behavior will be discussed further.

The properties of real gases are easier to understand if they are discussed in terms of deviations from ideal behavior, which in turn is simply a statistical description of the properties of a collection of non-interacting particles. A very good example of such a treatment is the virial expansion for an imperfect gas.[15] The virial expansion for a binary gas mixture was derived in chapter II, Part I, as equations (I-11)-(I-37); the result for a single component gas is (see also equations (I-62)-(I-66))

$$P/kT = \rho + B_2(T)\rho^2 + B_3(T)\rho^3 + \ldots = \rho + \sum_i B_i(T)\rho^i \qquad (II\text{-}1)^*$$

where P is the hydrostatic pressure, k is the Boltzmann constant, T is

---

*Equation numbers in Part Two will be preceeded by Roman numeral II.

the absolute temperature, ρ is the density N/V, and the B_i are the virial coefficients which are related to the i particle configuration integrals; see, for example, equations (I-34), (I-35), and (I-36).

In the limit as $\rho \to 0$, equation (II-1) reduces to the ideal gas equation. The additional terms then represent deviations from ideality which are caused by molecular interactions. For instance, according to equation (I-36), B_2 is an integral over the additional energy levels which may be occupied as a result of the interactions between just two molecules. Now, as the gas density increases, pair and higher interactions become increasingly important in determining the properties of the gas, just as the higher terms in the series (II-1) then reflect greater deviations from ideal properties.

In order to determine the effects of molecular interactions on gas behavior, imagine first a collection of non-interacting particles of infinitely small size. The equation of state is the ideal gas equation. If these particles are given a finite size, then part of the volume of their container is no longer accessible; it is occupied by other molecules. The ideal gas equation does not hold, because the container volume no longer describes the accessible volume; actually, there are fewer energy states available to the molecules. Now imagine that dispersion interactions occur between these particles. These interactions are always attractive, meaning that close together configurations of molecules represent states of lower potential energy. This means that additional energy states may become accessible, with the result that the molecules will spend more time in close proximity to one another.

Whether or not more states become accessible depends on the temperature. Thus at high temperatures, dispersion interactions do little to effect gas properties; deviations from ideality are, however, caused by the excluded volume of the molecules. $B_2(T)$, for example, would in this situation be positive. As the temperature is lowered, the molecules tend to pack together; the resulting behavior is as if more volume became accessible to the system (that is, the number of accessible energy states is greater than that predicted by the container volume), and $B_2(T)$ becomes negative.

This imagined experiment is in many ways similar to volumetric physical adsorption experiments. The pressure, temperature, and volume of a sample of adsorbate gas is carefully measured. Assume that equation (II-1) is the equation of state for the gas, with the B_i accounting for dispersion interactions between the gas molecules. The number of moles in the sample can be calculated by first multiplying equation (I-64) by V, then:

$$PV/kT = \sum_{j \geq 1} Vb_j(f/kT)^j \qquad \text{(II-2)}$$

Substituting this relation into equation (I-13) gives

$$\bar{N} = \sum_j jVb_j(f/kT)^j \qquad \text{(II-3)}$$

where the b_j are related to the virial coefficients of equation (II-1); see for example equation (I-26).

Next, this dose of gas is physically allowed access to the adsorbent, and the pressure, temperature, and volume are carefully measured again. The number of moles is recalculated, and may be found to be less than what was in the original dose. This is because if the gas-solid interactions are large enough, then some gas molecules will spend much of their time close to the adsorbent; these are effectively removed from the gas phase, and are said to be adsorbed.

Imagine, however, that additional gas was added to the system so that the fugacity was the same as before the adsorbent was introduced. The correct virial expression will still accurately describe the number of moles in the system, even when the adsorbent is present:

$$\bar{N}' = \sum_{j \geq 1} jVb_j' (f/kT)^j \qquad \text{(II-4)}$$

where the b_j' also includes the gas-solid interactions. Then the number of moles which are adsorbed is given by

$$\bar{N}_a = \bar{N}' - \bar{N} = \sum_j jV(b_j' - b_j)(f/kT)^j \qquad \text{(II-5)}$$

This may be rewritten as[16]

$$\bar{N}_a = \sum_j B_j + 1, s(f/kT)^j \qquad \text{(II-6)}$$

where, for example, B_{2s} is the second gas-solid virial coefficient and results from the interaction of just one molecule with the entire solid.

The configuration integral for B_{2s} may be solved if some potential function is assumed for U_{1s}. It has been shown that the Lennard-Jones (3-9) potential function adequately describes this interaction; the configuration integral may then be solved to give[17]

$$B_{2s} = Az_0 \sum_{\tau = 0}^{\infty} (9\tau!)^{-1}[(3\sqrt{3}\varepsilon'_{1s}/2kT)]^{(6\tau + 1)/9}\Gamma[(3\tau - 1)/9] \qquad (II-7)$$

where A is the adsorbent surface area, z_0 is the distance where the gas-solid potential is zero, ε'_{1s}/k is the minimum in the gas-solid (3-9) potential function, and $\Gamma[(3\tau - 1)/9]$ is the gamma function. If B_{2s} is determined at several temperatures, Az_0 and ε'_{1s} may be determined from the set of such values which, when used in equation (II-7), give the best agreement with experimental values.

The purpose of this work was to investigate the adsorption properties of krypton on the (1, 1, 0) surface plane of single crystals of copper. The results are to be analyzed by the virial treatment, to yield values of Az_0 and ε'_{1s}. These results are then to be compared with the results of Carden's work[17,18] with the adsorption of krypton on the (1, 1, 1) crystals. Since the only significant difference between these two adsorbents is the geometry of their surface atoms, this aspect should now be discussed.

The packing of surface atoms in the (1, 1, 1) and (1, 1, 0) plane is shown in figures 9A and 9B. The atoms in the (1, 1, 1) plane are closest packed and are 2.55 Å apart. The packing in the (1, 1, 0) plane consists of rows of copper atoms; the atoms within a row are 2.55 Å

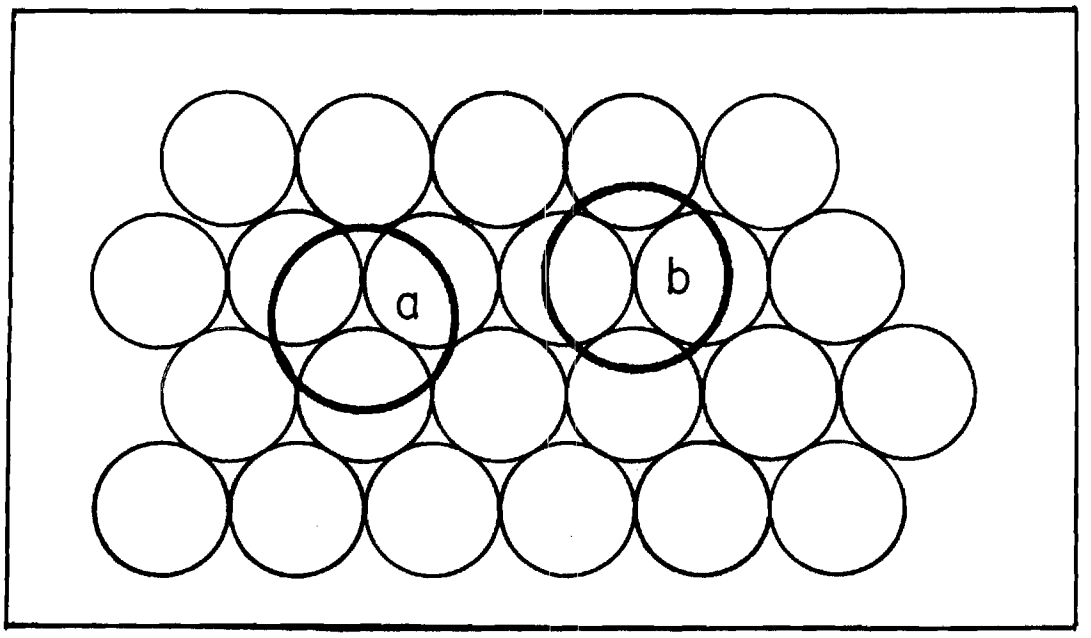

9A. The arrangement of atoms on the (1, 1, 1) surface

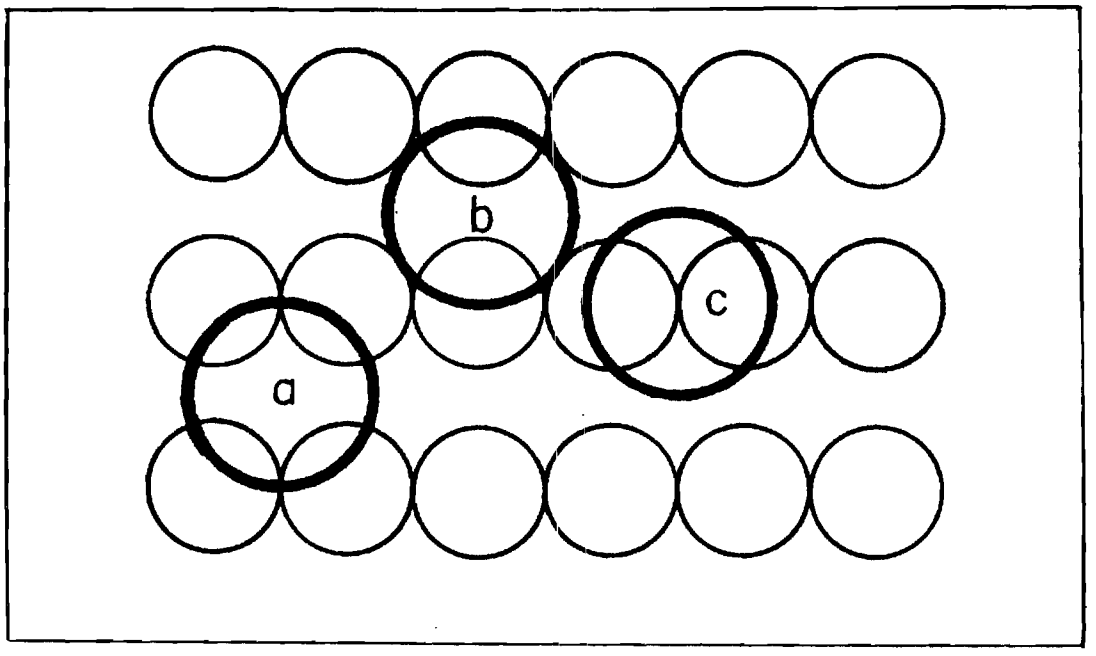

9B. The arrangement of atoms on the (1, 1, 0) surface

Figure 9. The Arrangement of Atoms on the (1, 1, 1) and (1, 1,0) Surfaces

apart, and the rows themselves are 3.62 Å apart. Since the hard sphere diameter of a krypton atom, 3.67 Å, is roughly the same as these dimensions, it might be expected that the surface structure could influence adsorption behavior.

Non-metallic adsorbents are often treated as collections of individual atoms, and lattice summation techniques may be employed to describe the gas-solid interaction. Metals are often treated as if the surface were smooth and homogeneous, since the lattice spacing is small compared to the equilibrium distance between the adsorbate and the metal surface, which for example, has been reported to be about 3.77 Å for the adsorption of krypton on a copper (1, 1, 1) surface.[18,19] In such treatments, the adsorbate is assumed to interact with a homogeneous surface that has a density equal to the average atomic density of the particular surface structure. Since the distance of closest approach is taken to be the same for each surface, the interaction energy is always found to be lower for the less dense faces; or, for example, $\varepsilon'_{ls}(1, 1, 1)$ should be greater than $\varepsilon'_{ls}(1, 1, 0)$.

Kaspersma[19] has applied several such treatments to describe the adsorption of argon, krypton, and xenon on three faces ((1, 1, 1), (1, 1, 0), and (1, 0, 0)) of nickel and copper. In particular, he finds a minimum in the adsorption potential equal to 1628°K for the adsorption of krypton on copper (1, 1, 1) and a value of 1452°K for krypton adsorption on copper (1, 1, 0).

It was decided that some estimate of the effect of the structure of metal surfaces could be obtained through a lattice summation

calculation. The method of calculation was to generate the lattice positions of some number of copper atoms, with a lattice spacing calculated from the density of copper. An atom at each of these positions then interacts according to the Lennard-Jones (6-12) potential with the adsorbate atom, which is located at a known position relative to the lattice. The collision diameter, σ_{Kr-Cu} is taken to be $(\sigma_{Kr} + \sigma_{Cu})/2$, where σ_{Cu} is varied until a potential function for the interaction of krypton with the (1, 1, 1) face of copper is obtained which has a minimum occurring at 3.77 Å, an experimental value determined in the previous studies. The value of σ_{Cu} found in this manner was 3.89 Å. Since the dispersion interaction of krypton with the individual copper atoms in the metal is not known, a reduced quantity is calculated:

$$U/\varepsilon_{Cu-Kr} = \Sigma\, 4[(3.89/r)^{12} - (3.89/r)^{6}] \qquad \text{(II-8)}$$

The metal, then, is considered to be a collection of 3.89 Å spheres, closest packed in a lattice structure, and spaced every 2.55 Å (the lattice spacing for copper). Since the atomic diameter is greater than the distance between lattice positions, the surface structure becomes smoothed out. The results are shown in figure 10, where five potential curves are given which were calculated by fixing the adsorbate coordinates which were parallel to the plane of the surface. Then only the distance from the surface is varied, and the adsorbate moves directly up or down over the sites indicated in figure 9A and 9B. Notice that site b in figure 9A and site c in 9B are similar, and that their

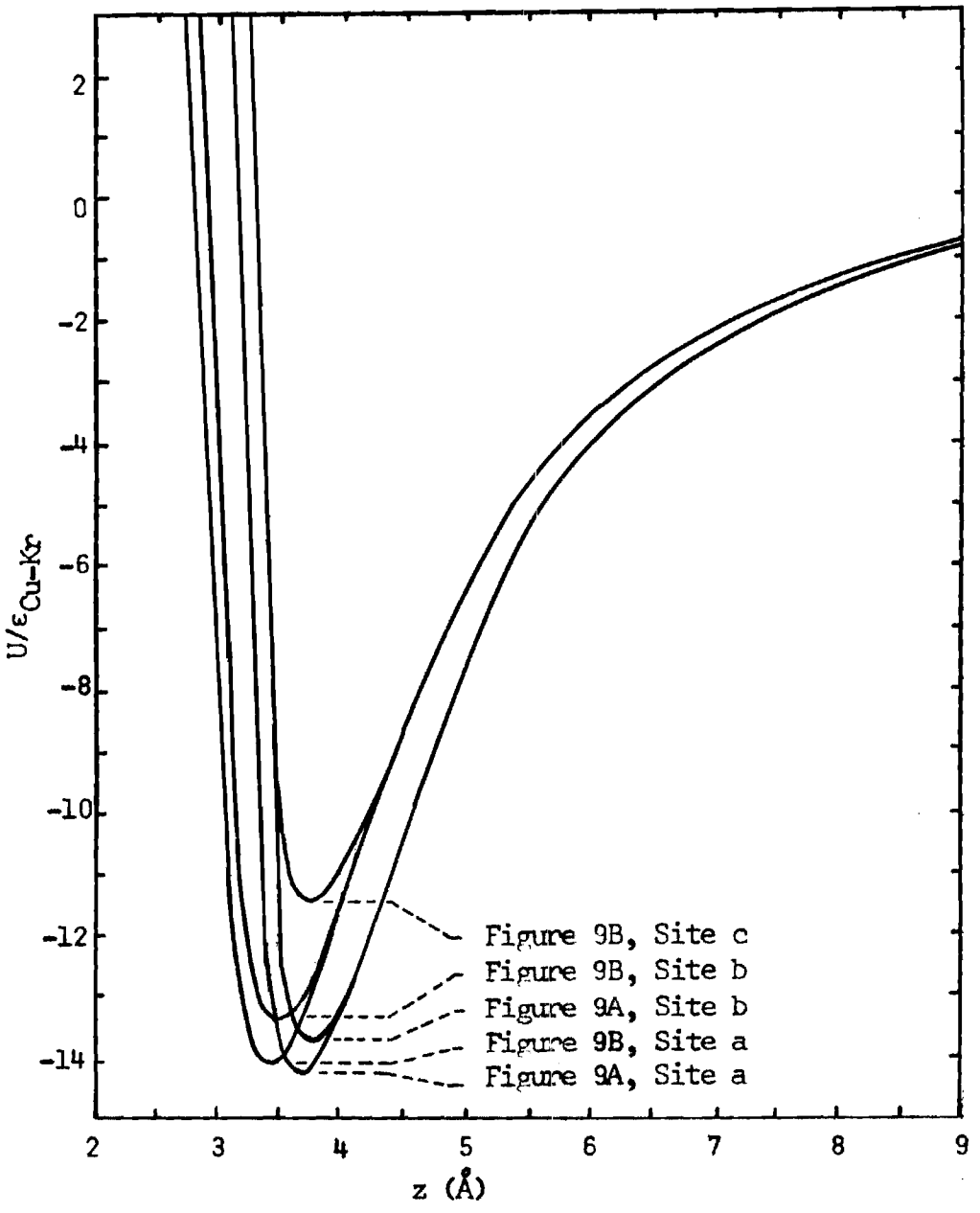

Figure 10. The Reduced Potential as a Function of the Distance between a Krypton Atom and a Copper (1, 1, 1) or (1, 1,0) Surface

potential minima in figure 10 occur at the same distance from the surface; but the interaction energy is much lower on the (1, 1, 0) surface. This is due to the less dense packing of the (1, 1, 0) surface atoms. However, the fact that it is a less dense structure means that the adsorbate atom may be able to fit in between the surface atoms. Curves 3 and 4 in figure 10 are a result of this; note that their potential minima occur at closer distances to the surface. Because of this, the interaction energy is much higher over these sites. Note also that the adsorbate is at a close distance to four copper atoms at site a, figure 9B, while an adsorbate on the (1, 1, 1) surface can contact a maximum of only three surface atoms.

According to this model, the maximum interaction of krypton with the (1, 1, 0) surface of copper should be roughly the same as for the maximum interaction with the (1, 1, 1) surface; however, the fraction of the (1, 1, 0) surface which exhibits such sites is much lower than for the (1, 1, 1) surface.

One other interesting feature should be noted. First note that the reduced interaction parameter U/ε_{Cu-Kr} has a minimum value of -14.35 at 3.77 Å on the (1, 1, 1) surface. Carden reports a value of 1678°K for ε'_{ls}/k in his study, so that if ε_{Cu-Kr}/k is taken to be 117°K, the lattice calculation will agree with Carden's data. From appendix B, the difference in reduced energy between sites a and c on the (1, 1, 0) face is $\Delta U/\varepsilon_{Cu-Kr} = 2.6$, or $\Delta U/k = 304°K$. At adsorption temperatures on the order of 90°K, it would therefore be expected that most krypton atoms would not be able to pass over the rows of copper atoms. However, as

the difference in reduced energy between sites a and b is relatively small (76°K), the krypton atoms should be able to move freely in between two rows.

The following chapters describe the equipment used in this study and give some experimental details. The results are analyzed by the virial treatment and compared with previous results.

CHAPTER II

EXPERIMENTAL

This section concerns the experimental aspect of physical adsorption, and describes the various pieces of equipment which are used, the growth and characterization of the single crystals of copper, and how the equipment is used to make the isotherm measurements.

Equipment

A volumetric adsorption apparatus, designed and used to obtain isotherms for the copper (1, 1, 1) - krypton system,[17] was available for use in this study. The number of moles of adsorbed gas is found by taking pressure, volume, and temperature measurements of the adsorbate before and after it comes in contact with the copper. Any apparent loss in the amount of gas after contact with the adsorbant represents the amount adsorbed. The following should serve as a description of the equipment, including some modifications that were made to it.

Vacuum System

An adsorbent surface must naturally be clean; free of any adsorbed contaminants. Metal surfaces have a high affinity for the residual gases usually found in vacuum systems. Consequently, an ultra-high vacuum environment is necessary to insure that a clean metal surface stays clean.

The vacuum equipment was constructed entirely of glass and metal

parts. Glass was sealed to kovar, metal-metal seals were made either by welding or brazing, or by using Granville-Phillips "Conflat" flanges or Cajon "VCR" couplings, both of which used metal (copper or nickel) gaskets, and, finally, all valves were Granville-Phillips ultra-high vacuum valves.

A Granville-Phillips model 225 pumping station, consisting of a Welch Duo-seal forepump and a liquid nitrogen trapped triple stage diffusion pump charged with Dow Corning 705 silicone fluid (a very low vapor pressure fluid; at room temperature its vapor pressure is $\sim 10^{-10}$ torr), was used to pump the system. The system has been pumped down to 8×10^{-10} torr, but pressures in the mid 10^{-8} torr range were the lowest that were routinely accessible. These pressures were measured by a Veeco RG75P ionization gauge, a hot cathode (iridium filament) type.

A schematic of the vacuum system used in this study is shown in figure 11, and differs from the original system in that a quadrupole mass spectrometer head has been added, and gases other than krypton which were let into the system at valve 6 are now let in through valve 3. This second modification was made when the mass spectrometer revealed that the original vacuum system was being contaminated with long chain hydrocarbons, the source of which was found to be the grease used in a manifold with stopcocks. Although the manifold was generally sealed from the rest of the vacuum system, it had to be pumped out through it. The present set up includes a separately pumped manifold with a bakeable charcoal trap, which is connected to the vacuum system at valve 3. Gases admitted through this manifold were found to be clean and did not

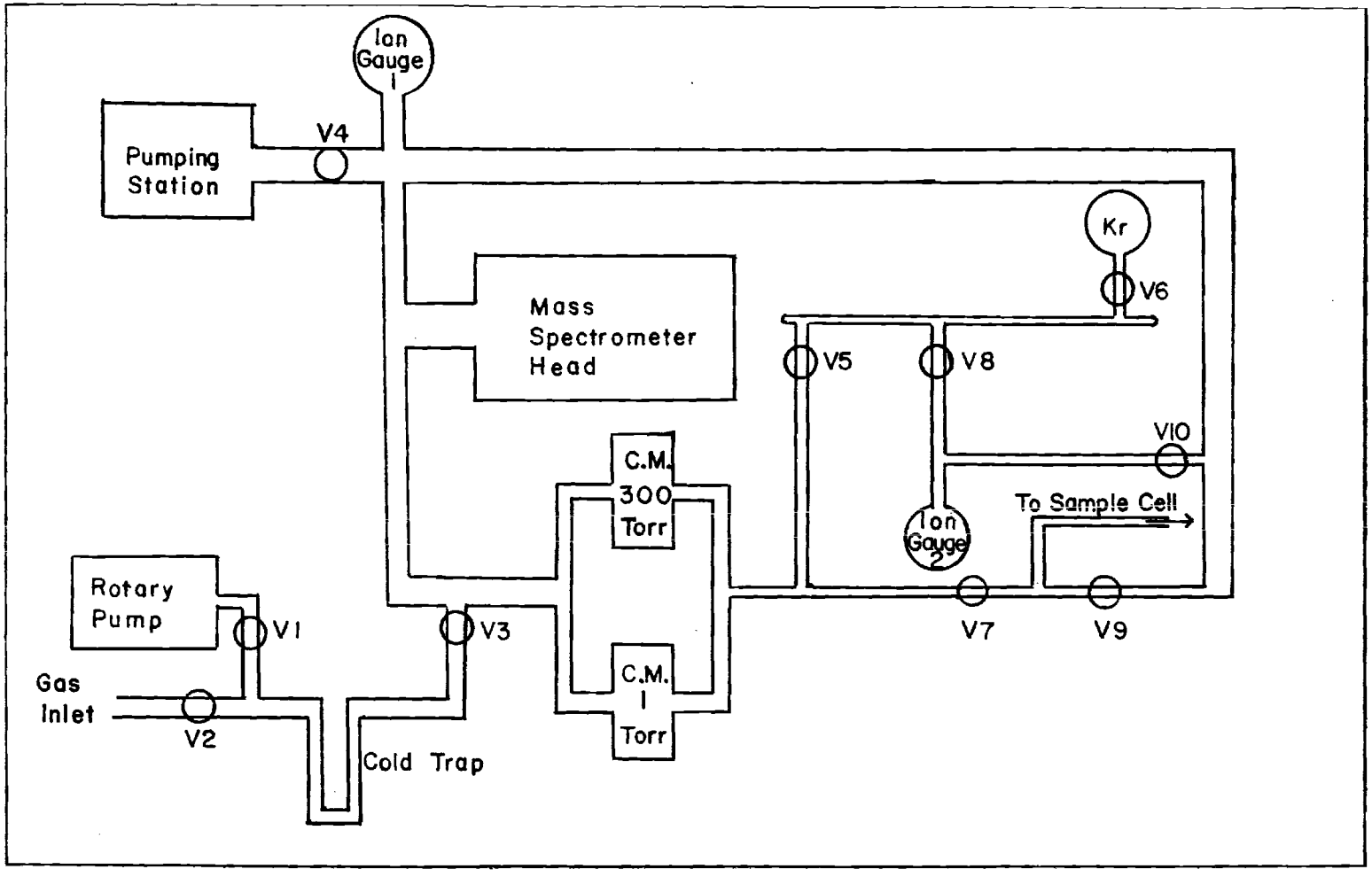

Figure 11. Schematic of Vacuum System

contaminate the vacuum system.

Most of the high vacuum section (excluding the sample cell, pumps, and an external manifold) was enclosed by an insulating asbestos fiberboard and could be baked at 250°C by means of two 1 Kw radiant heaters. In order to prevent possible damage to some of the equipment, it was generally preferable to raise the temperature to only about 110°C for around five hours. This would result in a subsequent pressure in the mid 10^{-8} torr range, if, as was usually the case, the system was not previously contaminated with hydrocarbons. The residual gases were principally water and carbon monoxide.

Capacitance Manometer

Volumetric adsorption techniques require accurate measures of the adsorbate pressure in order to find out how much adsorbate remains as a gas. The low surface area of the copper adsorbent and a relatively large dead space volume means that only a small amount of the total gas present should be adsorbed; the exact amount will then have to be found from the difference between two large numbers.

An MKS "Baratron" capacitance manometer gauge, equipped with a model 90H-1 head, was used to measure the adsorbate pressure. The 90H-1 head was entirely welded, made of metal and glass, and fully compatible with ultra-high vacuum equipment. It could measure a differential pressure of up to 1 torr (it could withstand one atmosphere); the gauge readout could be expanded through eight ranges, from 3×10^{-4} to 1 torr full scale. This particular pressure head had been calibrated by the manufacturer, and a table of such data was supplied with it. The

calibration corrections were always applied to the raw data.

A 90H-300 head was attached to the system, but was not used.

Temperature Measurement

Temperature measurements were made by measuring the potentials of copper-constantan thermocouples. The previously used Leeds and Northrup type K-2 potentiometer was replaced for this study by a Leeds and Northrup type K-3 potentiometer.

Data from the International Critical Tables were used to convert the thermocouple EMF to temperature, for temperatures down to about 80°K; however, this was not a sufficient range for the cryostat thermocouples, since temperatures could be between 68°K and 110°K.

Between 68° and 113°K, the thermocouples were calibrated as follows. A dose of krypton, sufficiently large to insure that condensation would occur, was admitted to the cooled sample cell. The potentials of the thermocouples and the vapor pressure of krypton (using the 90H-1 head) were recorded. From published krypton vapor pressure data,[20] these potentials could be related to the absolute temperature. This procedure was repeated for nine temperatures between 68° and 75°K. A single point at 77.12°K was obtained when the thermocouples were immersed in liquid nitrogen boiling at an atmospheric pressure of 738.1 torr. The temperature of the liquid was found from the following equation for the vapor pressure of nitrogen:

$$T(°K) = 255.82/(6.4959 - \log_{10} P_{mm}) \qquad \text{(II-9)}$$

where T(°K) is the absolute temperature and P_{mm} is the vapor pressure in mm of mercury. Finally, from 80° to 113°K the International Critical Tables were used to relate thermocouple potentials to the absolute temperature. The data from these three sources was then found to fit the following equation, good for cryostat temperatures between 68° and 113°K:

$$T(°K) = 1576.533 + 817.533(EMF) + 160.505(EMF)^2 + 11.1797(EMF)^3 \quad \text{(II-10)}$$

Mass Spectrometer

The residual gas analyzer used here was a series 200 Electronic Associates, Inc. quadrupole mass spectrometer, with ranges of 1-50, 10-150, and 50-500 atomic mass/charge units. It was found to be very useful for monitoring the cleanliness of the vacuum system, the products of the oxidation and reduction treatments of the copper crystals (discussed later), and for finding the sources of leaks.

The higher mass ranges could provide a quick check on hydrocarbon or silicone oil contamination. If these were not present, the higher mass ranges would show no signal above m/e equal to about fifty; the lower mass range was used for identifying the presence of water, carbon monoxide, and carbon dioxide. The presence of an oxygen peak would immediately indicate that there was a leak in the vacuum system.

In the event there was some leak, the mass spectrometer would be set in a manual scan mode to detect only the mass of helium. The various parts of the vacuum system would then be sprayed with helium; when

the leak area was sprayed, the presence of helium would be quickly indicated by the spectrometer.

Cryostat

In order to calculate some of the thermodynamic quantities, the amount adsorbed must be known as a function of temperature. A cryostat had been constructed for this purpose, and could maintain a constant temperature bath for the sample cell to within 0.1°K between 78° and 110°K, when using liquid nitrogen. A schematic of the cryostat is shown in figure 12.

The temperature was regulated by means of controlling the vapor pressure of the liquid nitrogen. One end of a copper tube was sealed and inserted into the cryostat; the other end was connected to a U-tube mercury manometer, fitted with electrical contacts on one side. The copper tube could be filled with either oxygen (cryostat operation below 95°K) or methane (from a natural gas outlet); a rising cryostat temperature would increase the vapor pressure of either of these, resulting in a movement of the mercury column which might then meet an electrical contact. In that event, a valve would open which would vent the cryostat; the evaporating nitrogen would cool the bath and reverse the above process.

Some of the liquid nitrogen was constantly boiling away and had to be replaced. The cryostat did this automatically, with a level controller that operated much like the temperature controller. One end of a copper tube was sealed and inserted through the top of the cryostat until the tip was just at the desired liquid level. The other end was

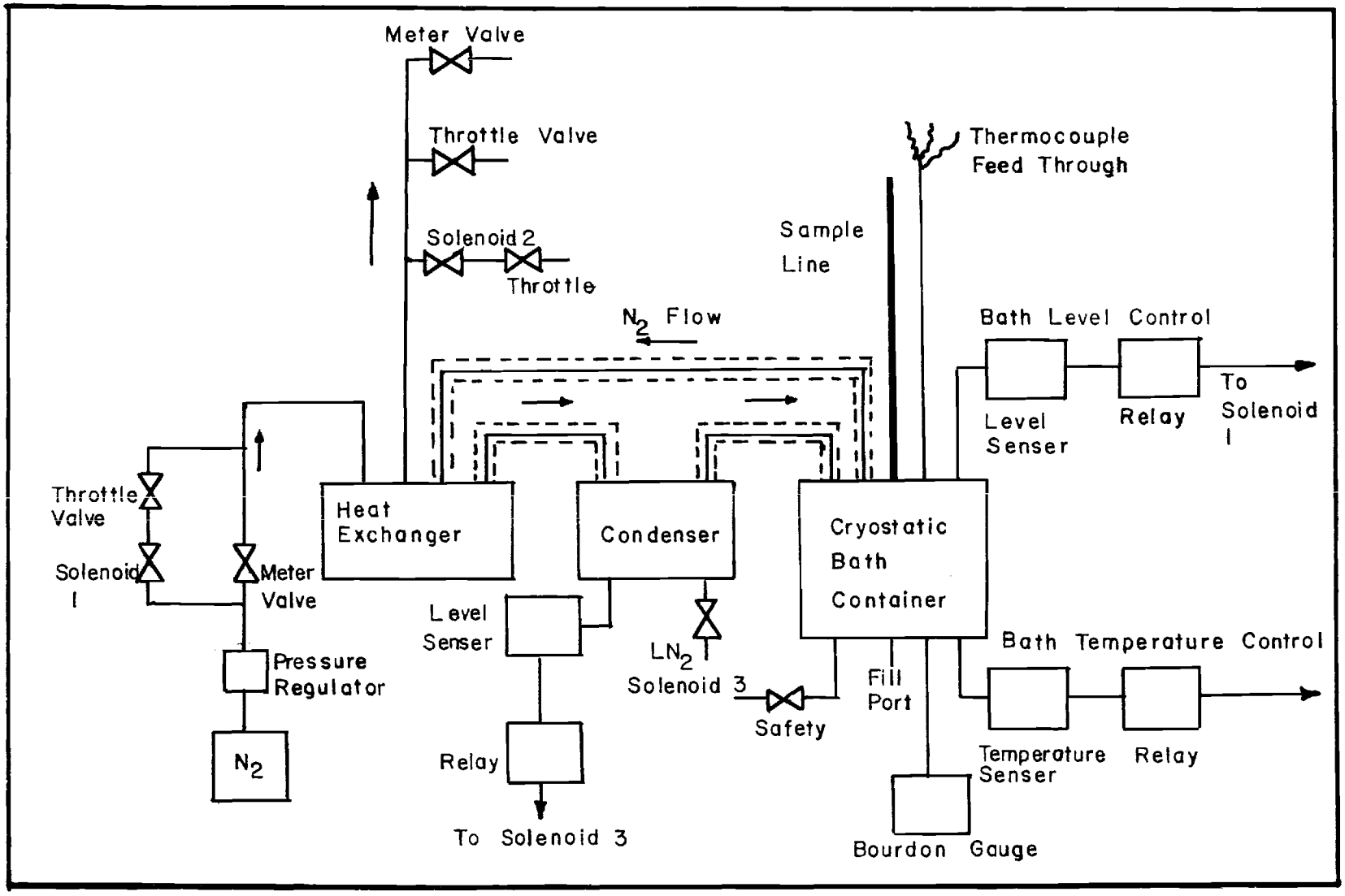

Figure 12. Schematic of the Cryostat (From Carden[18])

connected to a manometer similar to the one described above. When the liquid level falls below the tip of the copper tube, the rising vapor pressure of the gas sealed in it opens valve 1, figure 12, thus forcing liquid nitrogen to enter the cryostat from the condenser dewar. This condenser is an open dewar kept filled with liquid nitrogen, and contains a coiled copper tube, through which the gaseous nitrogen must pass before it enters the cryostat. Since the pressures in the cryostat are always greater than atmospheric pressure, the gaseous nitrogen condenses before it enters the cryostat and raises the liquid level.

The cryostat could not be filled directly from standard liquid nitrogen tanks, since at the time the cryostat was built, these had maximum operating pressures below those found in the cryostat. This is no longer true, and the cryostat could be easily modified to accept liquid nitrogen directly from a commercial tank.

It was decided to extend the range of the cryostat to include temperatures below 77°K (the boiling temperature of nitrogen at 1 atm.) so that the vapor pressure of krypton would fall below one torr, and then multilayer adsorption could be observed. This requires that the pressure in the cryostat be maintained below one atm; for this purpose a vacuum line containing a solenoid valve was installed between the cryostat and a 24 ft^3/min rotary vane vacuum pump. The solenoid valve replaces valve #2, so that the temperature regulator opens the line leading to the vacuum pump when the cryostat temperature starts to rise.

The operation of the bath level controller also had to be changed. Since the cryostat pressure was less than atmospheric pressure, no

liquid nitrogen would form in the condenser. Satisfactory operation was obtained by immersing another solenoid valve directly in a dewar of liquid nitrogen. This valve was attached directly to the cryostat by means of a short length of thick-walled rubber tubing, which served as a good thermal insulator. This valve then replaced solenoid valve #1 in figure 12, so that when the bath level falls too low, the immersed solenoid opens and liquid nitrogen is drawn into the cryostat. This operation would frequently cause the temperature to rise perhaps 0.3°K, since the incoming liquid nitrogen was warmer than that already present.

Sample Cell

During the isotherm measurements the copper crystals must reside in some leak-tight container attached to the vacuum system. This container must be able to withstand a temperature range of 70° to 650°K without leaking, and without contaminating the crystals. It should also have the smallest surface area and volume possible. Its inside surface characteristics should be reproducible and not change after, say, a bake-out performed in order to clean it up after exposure to the atmosphere. Finally, the material it is constructed of must be hard enough to crush a metal gasket and form a leak tight seal. The design of the cell is shown in figure 13; the cell was machined from a rod of solid nickel. The inside of the cell was electropolished using a 75 percent acetic acid and 25 percent perchloric acid electrolyte. The cathode consisted of a stainless steel tube suspended down the center of the cell, and was prevented from touching the bottom by means of a pointed teflon spacer.

In Carden's previous study, a very high roughness factor for the

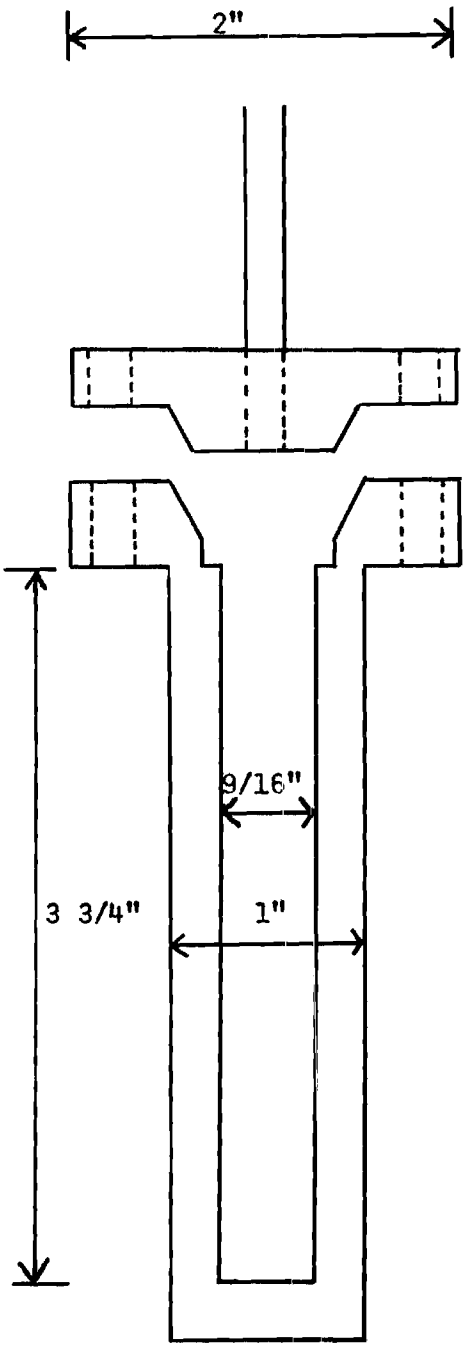

Figure 13. Diagram of the Sample Cell

empty sample cell was attributed to an oxidized stainless steel tube which connected the sample cell to the vacuum system. A copper tube had therefore been tried, but it developed cracks at silver solder joints and leaked. It was decided for this study to again use 1/8" O.D. copper tubing to alleviate the problem of a high roughness factor, and to use a gold-nickel brazing alloy at the solder joints. This arrangement also eventually leaked.

Nickel will form a reducible oxide film under the same conditions that stainless steel will form an irreducible film, but the smallest available nickel tube had an inside diameter of 0.46 cm., and would therefore contribute to an already large dead space volume. The final configuration settled upon was to use an eight inch length of nickel tubing soldered to the sample cell. The other end, which extends just beyond the top of the cryostat, was brazed with a gold-nickel alloy to a two foot length of 1/8" O.D. stainless steel tubing that attached to the vacuum system. This did not leak, and was expected to alleviate the problem of a high roughness factor for the cell.

The top of the cell was sealed to the bottom by means of a copper gasket. A piece of copper sheet was formed to fit between the top and bottom of the cell. This was trimmed and annealed, and was then placed again between the top and bottom of the cell. These were then bolted together with eight stainless steel bolts. Upon tightening of these bolts, a vacuum tight seal was formed.

Adsorption System

When isotherm measurements are being taken, only a part of the

vacuum system is used, and is sealed off by closing valves 8 and 9 in figure 14. This part of the system represents the volumetric adsorption system. All volumes within this part are accurately known, so that just pressure and temperature measurements will reveal the number of moles of gas residing in some particular volume.

In order to calibrate these volumes, a piece of equipment referred to as the primary calibrated volume, PCV, was attached to the adsorption system in place of the sample cell (see figure 12). The volume of the glass bulb of the PCV, V_{PCV}, was accurately determined by weighing the amount of mercury it took to fill it; the volume can be found from a knowledge of the density of mercury at the appropriate temperature. The volume of the PCV from the end of the Cajon fitting to the stopcock, V'_{PCV}, was also determined in this manner.

With the PCV in place, the entire system is evacuated through valve 9. Then valves 9 and 7 and the PCV stopcock are closed, and valve 5 is used to admit about 0.7 torr of helium into the gas pipet volume. This first step is concluded by recording the EMF of thermocouples 2, 3, and 4, and recording the pressure as P_1.

The second step consists of opening valve 7, and after the pressure has stopped changing, the potentials of thermocouples 2, 3, 4, and 5 are recorded, as well as the pressure, P_2.

Finally, the stopcock on the PCV is opened. The potentials of thermocouples 1, 2, 3, 4, and 5 are recorded along with the pressure, P_3.

This data can be analyzed to give the pipet volume and also the

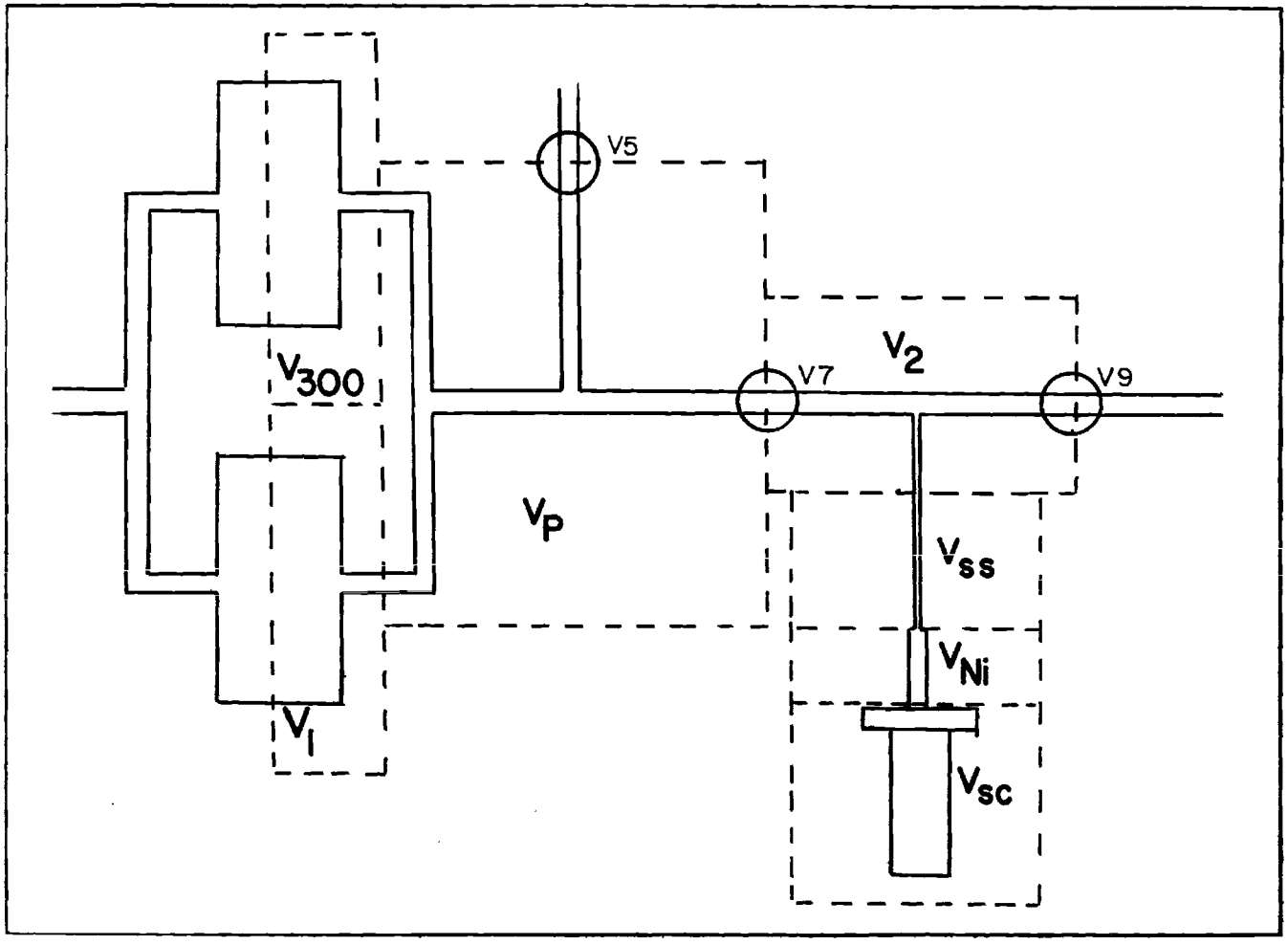

Figure 14. Diagram of the Adsorption System

volume denoted as V_2 (figure 14). The pipet volume includes the tubes leading to the two capacitance manometer heads, which are kept above the temperature of the rest of the system. It then becomes necessary to divide this volume into three separate regions, each maintained at a different temperature: V_1 for the volume which is maintained at the temperature of the 90H-1 head, V_{300} for the 90H-300 head, and V_p for the rest of the pipet volume. If the temperature given by thermocouple X during the $i^{\underline{th}}$ step is denoted by TX_i, then the number of moles of gas in the pipet volume in the first step is given by

$$n_1 = (P_1/R)[(V_1/T3_1) + (V_{300}/T2_1) + (V_p/T4_1)] \qquad \text{(II-11)}$$

The use of the ideal gas law under these conditions introduces less error than the experimental measurements.

The number of moles in the system in the second step is given by

$$n_2 = (P_2/R)[(V_1/T3_2) + (V_{300}/T2_2) + (V_p/T4_2) + ([V_2 + V'_{PCV}]/T5_2)] \qquad \text{(II-12)}$$

and in the final step

$$n_3 = (P_3/R)[V_1/T3_3) + (V_{300}/T2_3) + (V_p/T4_3) + ([V_2 + V'_{PCV}]/T5_3) + (V_{PCV}/T1_3)] \qquad \text{(II-13)}$$

Since the adsorption system is closed, $n_1 = n_2 = n_3$, and equation (II-11)

can be equated with equation (II-12) to give a relation between V_p and V_2. V'_{PCV} has already been determined, and V_1 and V_{300} were determined geometrically from data supplied by the manufacturer of the pressure heads. This relation can then be substituted into equation (II-13) to give either V_p or V_2 as the only unknown.

The sample cell is now attached to the system in place of the PCV. The volume of the tubing leading to the cell is determined by geometry, leaving the volume of the cell, V_{sc}, as the only one still undetermined. As before, the system is evacuated through valve 9, then a dose of helium is leaked into the pipet volume. The dose is measured and expanded into the sample cell, then measured again. This data can be analyzed to give V_{sc}. Table 6 gives the experimental values for the volumes discussed above.

Copper Crystals

Six single crystals of copper were grown for this study. Their dimensions were approximately 80 x 9 x 0.7 mm, and the broad face was parallel to the (1, 1, 0) plane. The crystals were grown using the Bridgemann technique, in which a graphite crucible, of the form shown in figure 15, is used. This crucible is filled with copper as shown, then sealed and placed in a furnace.

The furnace used here was borrowed from the Georgia Tech Engineering Experiment Station. It was specially designed by Dr. W. R. Livesay of the Georgia Tech EES for the purpose of growing metal crystals. Russell E. Eibling modified it and successfully grew several of the first (1, 1, 0) crystals.

Table 6. Volumes of the Adsorption System Shown in Figure 14.

Volume Designation	Volume (cm^3)
V_{300}	4.45
V_1	4.45
V_p	15.52
V_2	16.37
V_{ss}	0.70
V_{Ni}	2.65
V_{sc} (empty)	16.650
V_{sc} (with crystals)	13.402

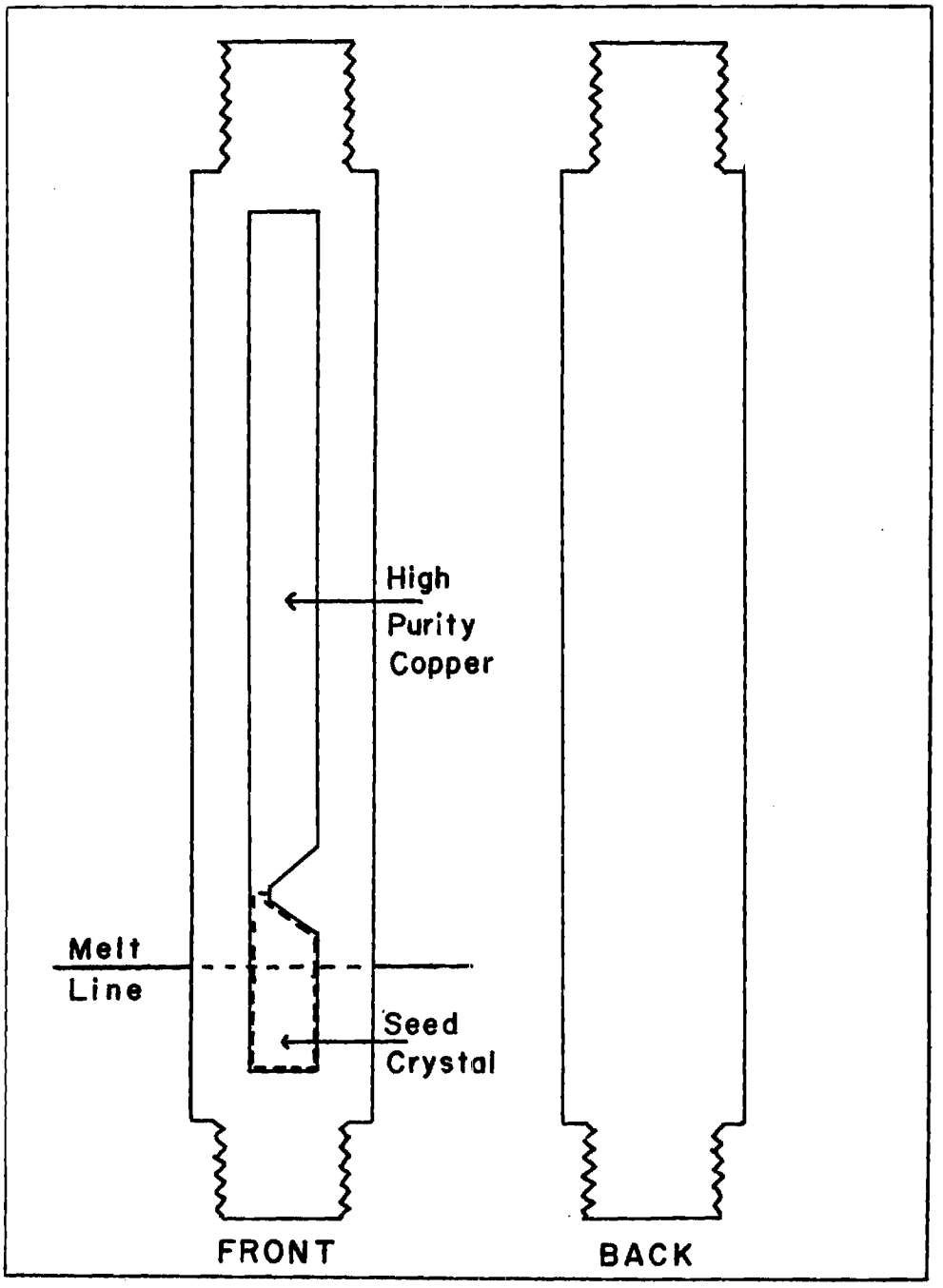

Figure 15. A Diagram of the Graphite Crucible Used to Grow the Copper Crystals. It consisted of a front and back piece which could be secured together by means of two threaded end caps.

The procedure used in growing the crystals is as follows. The crucible is placed in the furnace with the seed crystal at the bottom. The crucible is positioned so that the melt line falls just below the top of the seed crystal. The position of the melt line, previously determined by Eibling by trial-and-error methods, is where molten copper interfaces with solid copper when the furnace reaches its steady state temperature. With the crucible in position, the furnace chamber is evacuated and the furnace brought up to operating temperature. Typically, a vacuum in the 10^{-5} torr range could be maintained during crystal growth. The crucible is then slowly lowered out of the furnace, at a rate of two inches per hour, until the melt line clears the top of the new crystal.

The single piece of copper is then removed from the crucible and etched with cold, concentrated nitric acid. The crystal orientation was checked by observing acid etch patterns through a Zeiss metal microscope. These patterns are characteristic of the particular surface structure. For example, triangles are observed on the (1, 1, 1) face, squares on the (1, 0, 0), and rectangles on the (1, 1, 0) face.[21] Their formation depends on the fact that the nitric acid attacks different surface structures at different rates. The most dense packings (for example, the (1, 1, 1) structure) are attacked the slowest. Although acid etch patterns are sometimes difficult to observe, particularly on the (1, 1, 0) face, grain boundaries always show up clearly upon acid etching. If grain boundaries were observed, the new crystal was always rejected. If none were observed, the piece of copper was taken to be a single

crystal, with the orientation of the seed crystal. The rectangular etch pits characteristic of a (1, 1, 0) face also could be observed.

When it was decided to keep a crystal, a small jeweler's saw was used to cut off the seed portion. A block of graphite, with a groove machined in it, served to hold the crystal during this operation. The seed crystal could then be reused. A small hole was drilled near one end of the other crystal, so that it could be hung in the sample cell.

After acid etching, the surface of the crystal is very rough. It should be as smooth and as flat as possible, to insure that a maximum amount of the surface actually is parallel to the (1, 1, 0) plane. A procedure for obtaining a flat and shiny copper surface by electropolishing has been described,[22,23] and was used here. It consisted, basically, of attaching the crystal to a larger copper block which served as the anode. These were placed in an electrolyte in which a large surface area copper cathode was also immersed. The electrolyte was made by dissolving 10-15 grams of copper oxide in a liter of concentrated phosphoric acid. The anodic overvoltage on the crystal was monitored and maintained at 1.0 volts. Electropolishing was continued until the surface appeared to have the very shiny, relatively flat characteristics which were sought.

Procedure for Measuring Isotherms

The crystals had to have a clean surface before any isotherm measurements could be taken. Simply heating the crystals in a vacuum will drive off most of the likely contaminants, such as oxygen, carbon

monoxide, carbon dioxide, water, or some hydrocarbons. However, evidence obtained from Auger spectroscopy indicates that elemental carbon is an ubiquitous contaminant on metals, and that simple heating will not remove it. Removal on copper can be accomplished if the heating is done in the presence of some small amount of oxygen, in which case the carbon can be burned off. During this process, the crystals themselves might oxidize, so that a subsequent cleaning step should be a reduction with hydrogen. The details of this procedure will be given in the next chapter.

Cleaning the blank cell or the crystals by such an oxidation and reduction procedure just described releases much carbon monoxide, carbon dioxide, and water into the vacuum system. These take a long time to pump out, as they adhere well to the stainless steel or the glass components of the vacuum system. The next step, then, is to bake out the vacuum system and the sample cell together in order to achieve a pressure in the mid to lower 10^{-8} torr range. Subsequent bake-outs of the sample cell alone, after exposures to such low pressures for several days, would show some contamination by carbon monoxide. Consequently, before every isotherm, the cell was baked out at 250°-300°C for nearly an hour. This was a sufficiently long period of time, since carbon monoxide evolution had always ceased after about an hour.

The adsorption isotherm on the copper crystals cannot be obtained directly. The geometric surface areas of the crystals and of the inside of the sample cell were roughly equal, so that there should be roughly equal adsorption on both surfaces. An isotherm on copper must then be

found by running an isotherm on the sample cell when it contains the crystals and also when it is empty. The difference in the two isotherms represents adsorption on the crystals. Obviously, care must be taken to insure that the nature of the sample cell surface is the same in both situations, and so identical cleaning procedures are employed in preparation for each type of isotherm.

Once the adsorbent surface has been thoroughly cleaned, the isotherm measurements can begin. The cell, either empty or holding the crystals, will have just been baked out, and the background pressure should be in the mid to lower 10^{-8} torr range. The adsorption part of the vacuum system, detailed in figure 14, is now sealed off. The cryostat is filled with liquid nitrogen and brought to the desired temperature. If the crystals are in the sample cell, they will cool down very slowly, as they are suspended in a vacuum. To insure thermal equilibrium between the crystals and the nitrogen bath, about one torr of helium is admitted into the evacuated adsorption system and sample cell through valve 9, figure 5; valve 9 is then closed. (The helium is Assayed Reagent Grade (Air Reduction Sales Company); it was passed through an activated charcoal trap maintained at liquid nitrogen temperature before entering the vacuum system. This trap was so efficient at removing impurities that an equivalent size dose of hydrogen would not pass through it.) As the crystals cool, the helium pressure drops. The pressure is monitored, and when it stops changing, it is assumed that thermal equilibrium has been established.

The helium is then evacuated by opening valve 9. When the

background pressure drops to its previous level, then all of the helium has been pumped out and valve 9 is closed. Valve 7 is also closed, then valve 5 opened slightly to admit a dose of krypton into the gas pipet; then it is closed. When the pressure in the pipet becomes constant, it is recorded as the initial pressure, and the potentials of thermocouples 2, 3, and 4 are read to give the initial temperatures. The output of the capacitance manometer gauge is fed to a strip chart recorder, so that it is easy to tell when the pressure has settled to a constant value. Valve 7 is now opened, allowing the dose of krypton (the number of moles of which are now known by virtue of the data just taken) access to the sample cell. When the pressure again reaches a constant value, it is recorded as the final pressure, and the potentials of all of the thermocouples are recorded. This data will reveal the number of moles still in the gas phase after exposure to the adsorbent.

The next step is to close valve 7, then use valve 5 to admit more krypton into the pipet. The procedure given above is then repeated for this second dose. The adsorption measurements continue with additional doses until the final pressure in the cell is between 0.7 and 0.8 torr.

The number of moles of gas in the pipet volume before valve 7 is opened is given by

$$n_i = (P_i/R)[(V_{300}/T2_i) + (V_1/T3_i) + (V_p/T4_i)] \qquad \text{(II-14)}$$

where n_i is the initial number of moles, P_i is the initial pressure, and $T2_i$, for example, is the temperature given by thermocouple number 2 in

the initial phase of the dose, and V_{300}, V_1, and V_p are volumes defined in the last section.

Several complications arise when the final number of moles is calculated. Under operating conditions, there is a large temperature difference between the adsorbate pressure gauge and the sample cell. A large part of this thermal gradient is across the nickel tubing in the cryostat. Consequently, thermal transpiration corrections, according to the method of Miller,[26] were made for the pressures in the sample cell and in the nickel tube. Furthermore, the length of the nickel tube was divided into six separate temperature regions, and the stainless steel portion of the line to the sample cell was divided into two portions, one of which was effectively maintained at TR, taken to be about 280°K. If the final pressure that has been corrected for thermal transpiration is denoted as P_f^*, then an expression for the final number of moles of gas is

$$n_f = (P_f/R)[(V_{300}/T2_f) + (V_1/T3_f) + (V_p/T4_f) + ([V_2 + 0.789V_{ss}]/T5_f) + (0.211V_{ss}/TR)] + (V_{Ni}/R)[(4/13)(P_f^*/T1_f) + (1/26)(P_f^*/T(7-1)_f) + (2/13)(P_f^*/T7_f) + (3/26)(P_f^*/T(6-7)_f) + (2/13)(P_f^*/T6_f) + (1/26)(P_f^*/T(8-6)_f)] + P_f^*V_{sc}/RT8_f \qquad \text{(II-15)}$$

where $T(8-6)_f = T8_fT6_f/(T8_f + T6_f)$.

For the first dose, the number of moles adsorbed, n_a, is given by the difference between n_i and n_f. For all succeeding doses, the calculation of n_a is somewhat different because the dose is not expanded into

an evacuated cell. The number of moles remaining outside of the pipet volume when valve 7 is closed to get ready for the second dose is

$$n_{R,1} = n_{i,1} - (P_{f,1}/R)[(V_{300}/T2_{f,1}) + (V_1/T3_{f,1}) + (V_p/T4_{f,1})] \quad \text{(II-16)}$$

where the second subscript indicates the dose number.

In general, the number of moles remaining outside of the gas pipet in preparation for the $j^{\underline{th}}$ dose is

$$n_{R,j} = n_{i,(j-1)} - (P_{f,j}/R)[(V_{300}/T2_{f,(j-1)}) + (V_1/T3_{f,(j-1)}) + (V_p/T4_{f,(j-1)})] + \sum_{b=2}^{b=j-1} n_{R,b} \quad \text{(II-17)}$$

Finally, the number of moles adsorbed after the $j^{\underline{th}}$ dose is given by

$$n_{a,j} = n_{i,j} + n_{R,j} - n_{f,j} \quad \text{(II-18)}$$

CHAPTER III

RESULTS

This chapter describes the results of the cleaning procedure that was performed on the nickel cell and the copper crystals. The isotherms that were run on the clean metal surfaces are also given. Finally, these results are analyzed by the virial treatment discussed in the introduction.

Nickel Cell

Before any isotherms were run on the empty cell, it was cleaned according to the procedure given below. The oxygen and hydrogen were Assayed Reagent grade (Air Products Co.) which were passed through an activated charcoal trap maintained at dry ice temperature. When needed, these gases were leaked into the adsorption part of the vacuum system (see figure 14) which was then sealed. The pressure of the gases and the resulting reaction products were measured with the Baratron capacitance manometer.

The cell was cleaned by placing a heating coil around it and raising the temperature to 450°C (an iron-constantan thermocouple was used for these measurements). Large amounts of CO and CO_2 were initially driven off, but the outgassing became very slow after about one hour. It was observed that the CO began to desorb in significant amounts at about 250°C.

Next, valve 9 in figure 14 was closed, and about 0.5 torr of oxygen (the equivalent of several monolayers on the cell walls) was bled into the gas pipet by means of valve 5. Valve 7 was then opened, and the pressure dropped rapidly as the gas expanded into the sample cell. After that, the pressure at first fell slowly, then began to rise slowly. After approximately 30 minutes, valve 9 was opened in order to evacuate the cell and analyze the gaseous products, which were found to be CO, CO_2, and some O_2. Apparently, CO_2 is first formed, which then reacts with additional carbon to form CO, resulting in the slow pressure rise which was observed. This was checked by noting that the CO/CO_2 ratio always increased the longer the gas was kept in the hot sample cell.

After the cell was evacuated, the above procedure was repeated, but the oxygen gas was replaced by hydrogen. As before, the pressure dropped rapidly when the gas was first let into the cell. The pressure then fell slowly over a period of about an hour, at which time the pressure had fallen to about 0.03 torr. Apparently, the hydrogen had not found any oxides to react with and no water was formed; the nickel was apparently absorbing the hydrogen. The mass spectrometer subsequently revealed that a small amount of water had formed.

The cleaning process was repeated several more times, always with the same result. It appeared that there was always the same large amount of carbon present each time oxygen was admitted to the cell; the equivalent of about ten monolayers of carbon was actually removed.

It was decided at this time that only a reproducible cell surface,

not necessarily a clean one, was required. An isotherm should then be run, the cell cleaned again, and the same isotherm repeated to see if the surface changed as a result of the cleaning procedure. When this was done, it was found that the adsorption increased about two percent after the second cleaning, so the cell surface had changed very little, if any, since this was within experimental error.

Confident that a reproducible nickel surface could be obtained, four isotherms on the empty cell were run at 79.0°, 90.8°, 100.7°, and 107.7°K. These are shown in figure 16.

The following BET equation, given by Brunaur, Emmett, and Teller,[24] can be used to find the surface area of the adsorbent:

$$X/V_a(1 - X) = [1/V_mC] + [(C - 1)X/V_mC] \qquad \text{(II-19)}$$

where $X = P/P_0$ (P is the hydrostatic pressure of the adsorbate and P_0 is its vapor pressure), V_a is the volume adsorbed under the conditions of standard temperature and pressure, and V_m is the volume of adsorbed gas which would comprise one monolayer. This last quantity can be found from a plot of $X/(V_a(1 - X))$ vs X; then $V_m = (\text{slope} + \text{intercept})^{-1}$. The surface area can then be found from a knowledge of the area occupied by one adsorbate molecule when one monolayer is formed.

Using a value for the area of the krypton adsorbate as 14.6 $Å^2$, the BET area of the nickel cell was found to be 110 cm^2. As the geometric area of the cell was 49 cm^2, the roughness factor of the cell is then 2.25.

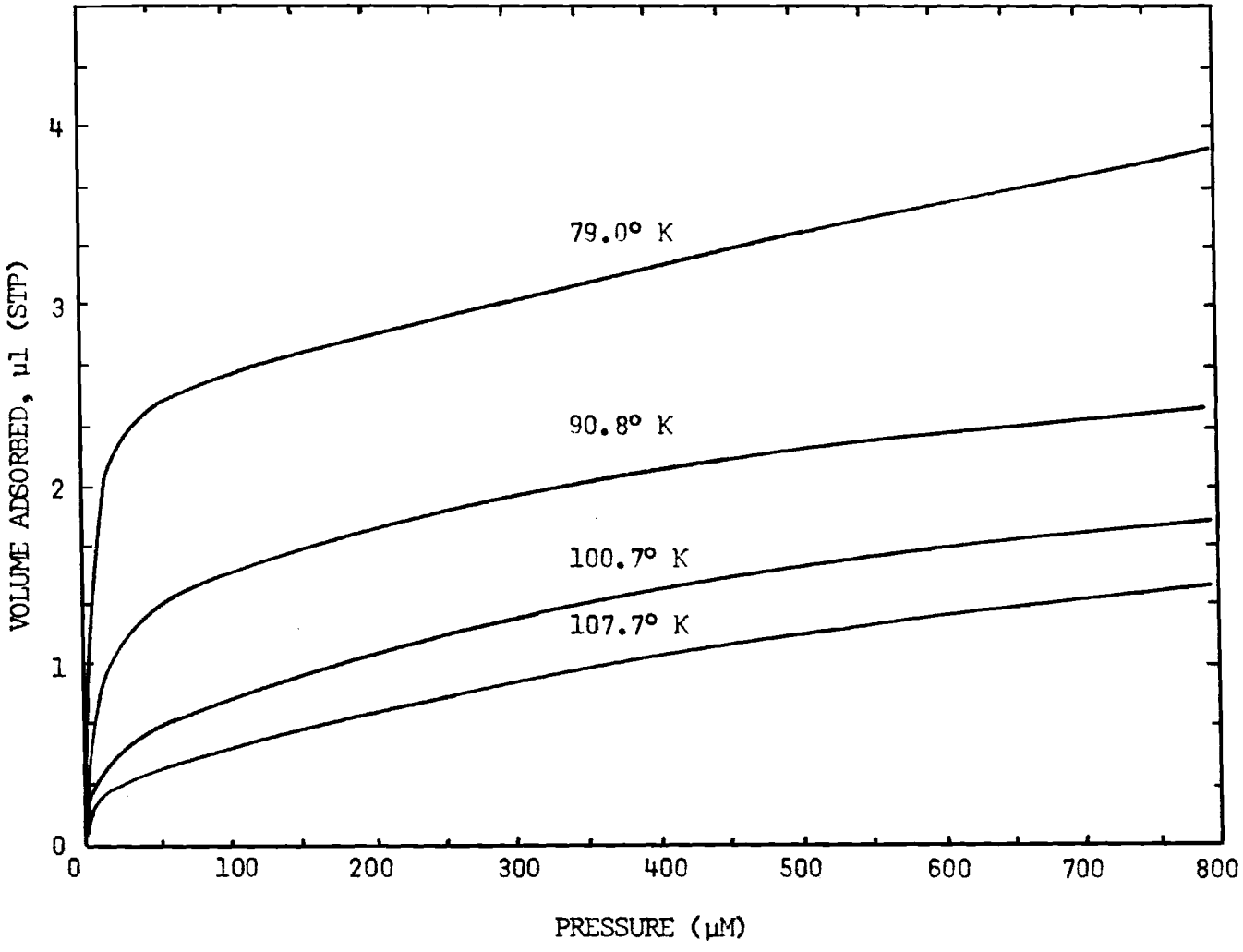

Figure 16. Isotherms on the Nickel Cell

Copper Crystals

It was decided to check out the instrument by reproducing Carden's earlier data. The sample cell was opened, but with great difficulty because the gasket had partially fused to the nickel. Six of the seven (1, 1, 1) copper crystals used earlier were placed in it. The cell was then sealed, evacuated and the cleaning precedure just described was begun. The cell was only heated to 350°C, to make subsequent opening of the cell easier. The cleaning behavior was different this time in that after several oxidation treatments, CO and CO_2 were no longer being formed. Instead, after several doses, the O_2 that was admitted to the cell was completely adsorbed. Subsequent reductions yielded much H_2O, indicating that the carbon had been removed from the cell, and that metal oxides were being formed in the oxidations.

The first isotherm was run on the apparently clean cell. The results are shown in figure 17. The difference between this isotherm and the isotherm on the empty cell is very much different from the isotherm on the (1, 1, 1) crystals reported by Carden. The crystals appeared now to have a very much higher surface area.

The cell was baked at a temperature of 450°C, then another isotherm was run, which resulted in an even higher adsorption than the first. A previous investigation into the interaction of copper (1, 1, 1) with krypton[23] had noted a similar difficulty; an apparent increase in surface area after a bakeout. In the previous study, the crystals were removed from the cell and etched with nitric acid. A peculiar etching on a small portion of one of the crystals was attributed

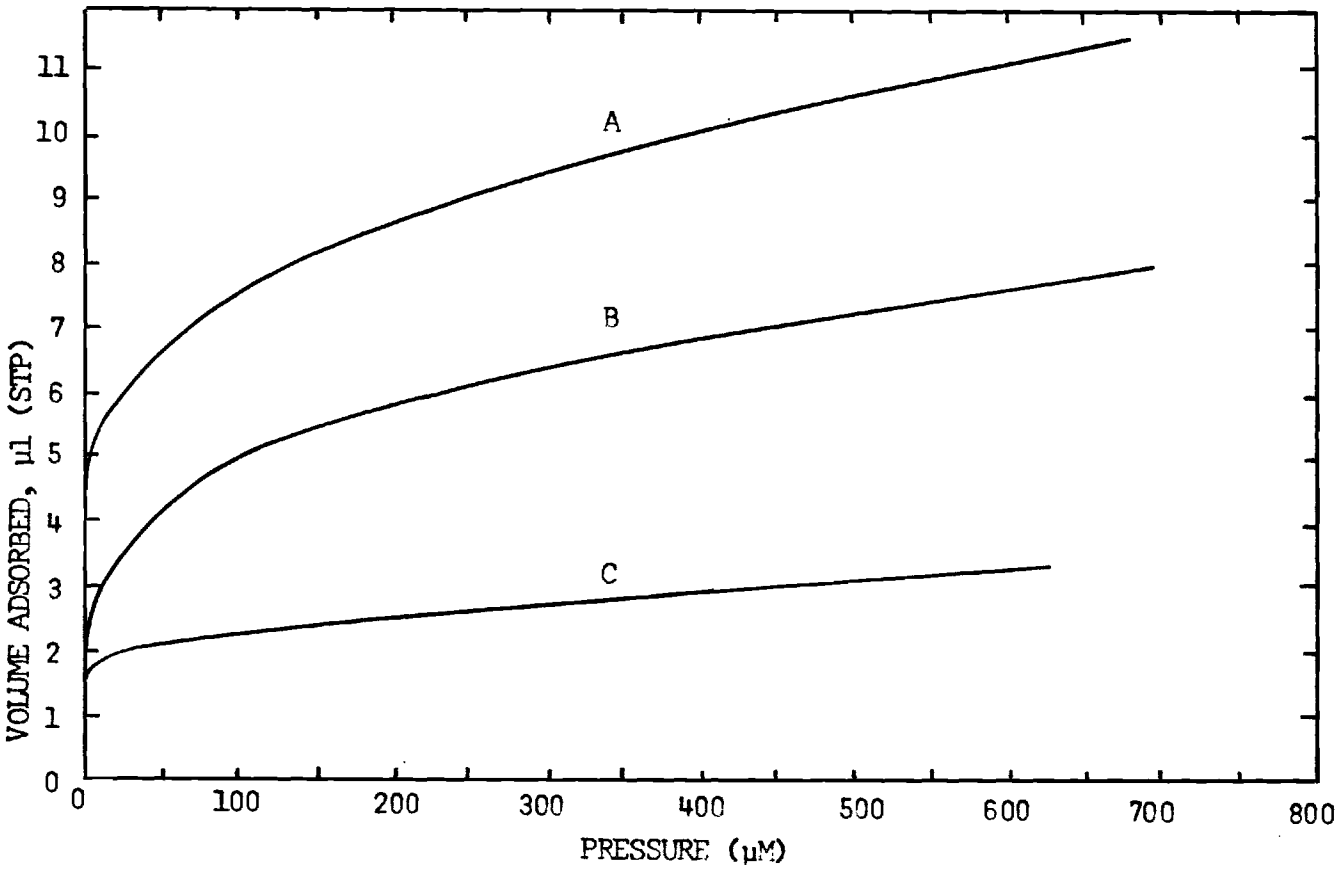

Figure 17. Adsorption Isotherms at 79.0° K. Curve A was the experimental result, curve C is Carden's result for the adsorption of krypton on copper (1, 1, 1). Curve B is the difference between curve A and the 79.0° K adsorption isotherm in Figure 16.

to contamination by silver solder flux, and this was taken to be the cause of the increased adsorption. In this study, the crystals were similarly removed and examined, but no contamination was found.

Further investigation of the problem revealed that copper readily sublimes in a vacuum (possibly requiring the presence of a small amount of H_2) at temperatures on the order of 300-350°C. A copper crystal was hung in an evacuated quartz tube, and then heated by means of an external resistance heating coil. When H_2 was leaked into the tube, the presence of a shiny copper film immediately became apparent on the walls of the quartz tube. Whether a copper oxide film, which would be more difficult to see, was present on the glass prior to the admission of H_2 is not known.

A close examination of the present condition of the nickel cell revealed that the surface was less shiny than before the crystals were placed in it, and that the surface had the appearance of being dusty. The cell was washed with distilled water, and the dusty material, apparently sublimed copper, was removed.

This second cleaning with the crystals present was apparently able to remove all of the carbon from the system, whereas the first one was not. It becomes clear that the nickel was the source of the carbon, and that it became covered with an evaporated copper film which was impermeable to carbon; furthermore, carbon could in fact be removed from copper.

The cleaning procedure was revised, hopefully to correct this problem. The oxygen or hydrogen gas are to be let into the cell at

room temperature, then about 500 torr of argon will be leaked in. The temperature should then be raised to about 350°C for 30 minutes, and then cooled. When the temperature has fallen below 275°C, the cell may be evacuated.

Isotherms on the cell with the crystals in it should be obtained first, so that the initial cleaning procedure will deposit a certain amount of copper on the cell wall (and possibly the new procedure will keep the amount to a minimum); subsequent bakeouts, until the crystals are removed, should then not exceed 250°C so that no additional amount of copper would sublime. Isotherms may then be run on the empty cell, which should still contain whatever amount of copper was deposited in it in the first place.

The copper (1, 1, 0) crystals described in the last section were now ready, so these were placed in the cell and cleaned according to the revised procedure. (Isotherms on the (1, 1, 1) crystals were not obtained.) Five krypton adsorption isotherms on the (1, 1, 0) crystals were then run at 72.8°, 79.9°, 92.2°, 101.6°, and 108.1°K.

The crystals were then removed, and the empty cell was cleaned by the revised procedure. Five more isotherms, at the same temperatures as before, were obtained.

The adsorption isotherms on the (1, 1, 0) crystals of copper were obtained at each temperature by subtracting the isotherm on the empty cell from the isotherm on the cell plus the crystals. This was done by drawing a smooth, best fitting line through each set of data points for each isotherm, and taking the difference between the smooth lines. The

resulting isotherms on the (1, 1, 0) face of copper are shown in figure 18.

Analysis of Results

BET Analysis

The BET analysis was applied to the 72.8° and 79.9°K isotherms, which resulted in surface areas of 89 and 75 cm^2 when using 14.6 $Å^2$ as the area per krypton atom. The geometric area was measured and found to be 89 cm^2, with approximately 7.5 cm^2 of that owing to edge area.

Virial Analysis

It was found in this study, as well as Carden's, that the linear portion of the isotherm does not extrapolate through zero (figure 19). This makes a straightforward application of the virial analysis impossible. The procedure used here was given by Thomas, Ramsey, and Pierotti,[25] and assumed that this additional adsorption could be described by the Langmuir equation:

$$n_a^h = n_m^h bP/(1 + bP) \qquad \text{(II-20)}$$

where n_m^h is the number of moles of adsorbate which would form a single molecular layer on the high energy surface responsible for the additional adsorption, b is a parameter related to the energy of adsorption, and P is the adsorbate pressure. Over the low coverage portion of an isotherm, for example that given in figure 19, the adsorption is determined by B_{2s}, and

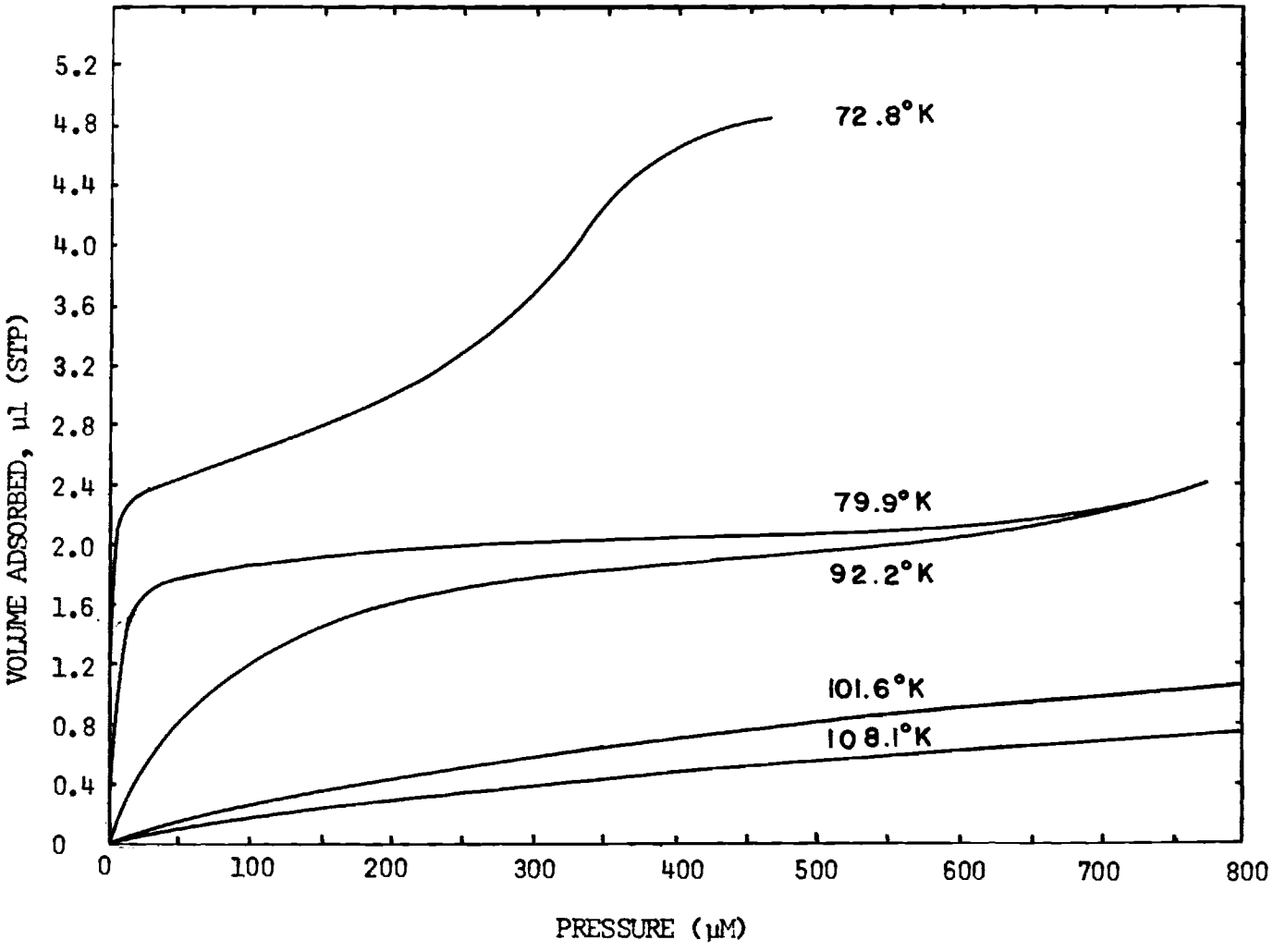

Figure 18. Adsorption of Krypton on Copper (1, 1, 0)

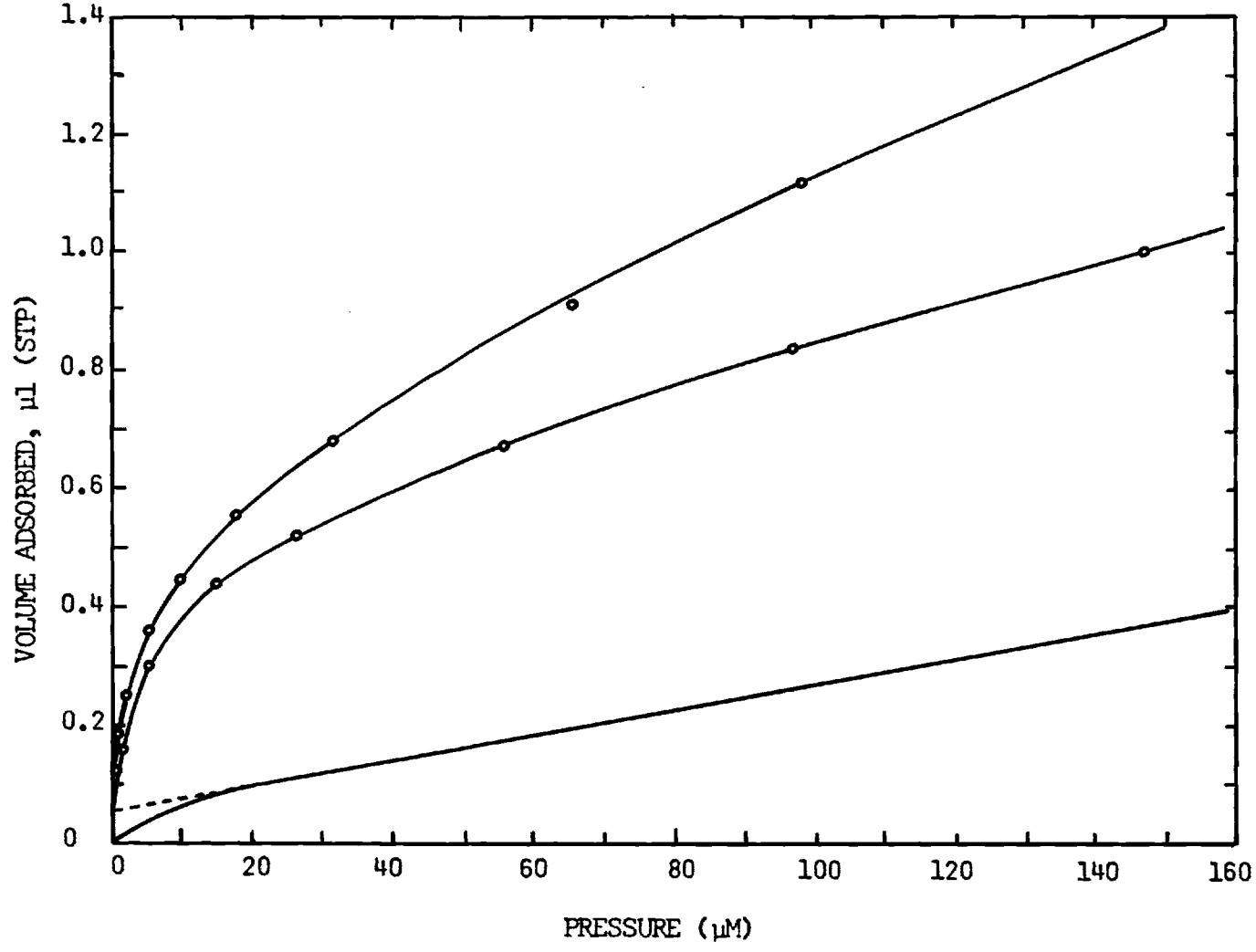

Figure 19. The Low Coverage Part of the 101.6° K Isotherms.

$$n_a = n_a^h + B_{2s}(P/RT) \qquad \text{(II-21)}$$

Values of n_m^h and b are chosen so that the resulting Langmuir isotherm, when subtracted from experimental data points, gives the best straight line. For example, the curve shown in figure 19 was broken down by this procedure into the two curves shown in figure 20. This procedure was repeated for the 108.1° and 92.2°K isotherms. These three values of n_m^h were then averaged, and the result was also used for the 79.9° and 72.7°K isotherms.

The slope of the straight line remaining after the Langmuir adsorption has been subtracted is the value of B_{2s}/RT. The experimental values of B_{2s}, n_m^h, and b are given in table 7.

This data was then fitted to equation (II-7); the best fit values were $\varepsilon_{ls}'/k = 1672°K$ and $Az_0 = 9.52 \times 10^{-7}$ cm^3. Figure 21 shows the experimental values, with the solid line given by equation (II-7). The goodness of the fit is indicated by the standard deviations between theoretical (equation (II-7)), and experimental values of $\ln Az_0$; for this data $\sigma \ln Az_0 = 0.30$.

Error Analysis

The uncertainty in the isotherm points could be estimated by first considering the errors associated with the temperature and pressure readings. These errors could then be applied to a set of experimental isotherm data points in such a way as to produce the largest change in the number of adsorbed moles. When this procedure was applied to the low pressure region of the 79.9°K empty sample cell isotherm,

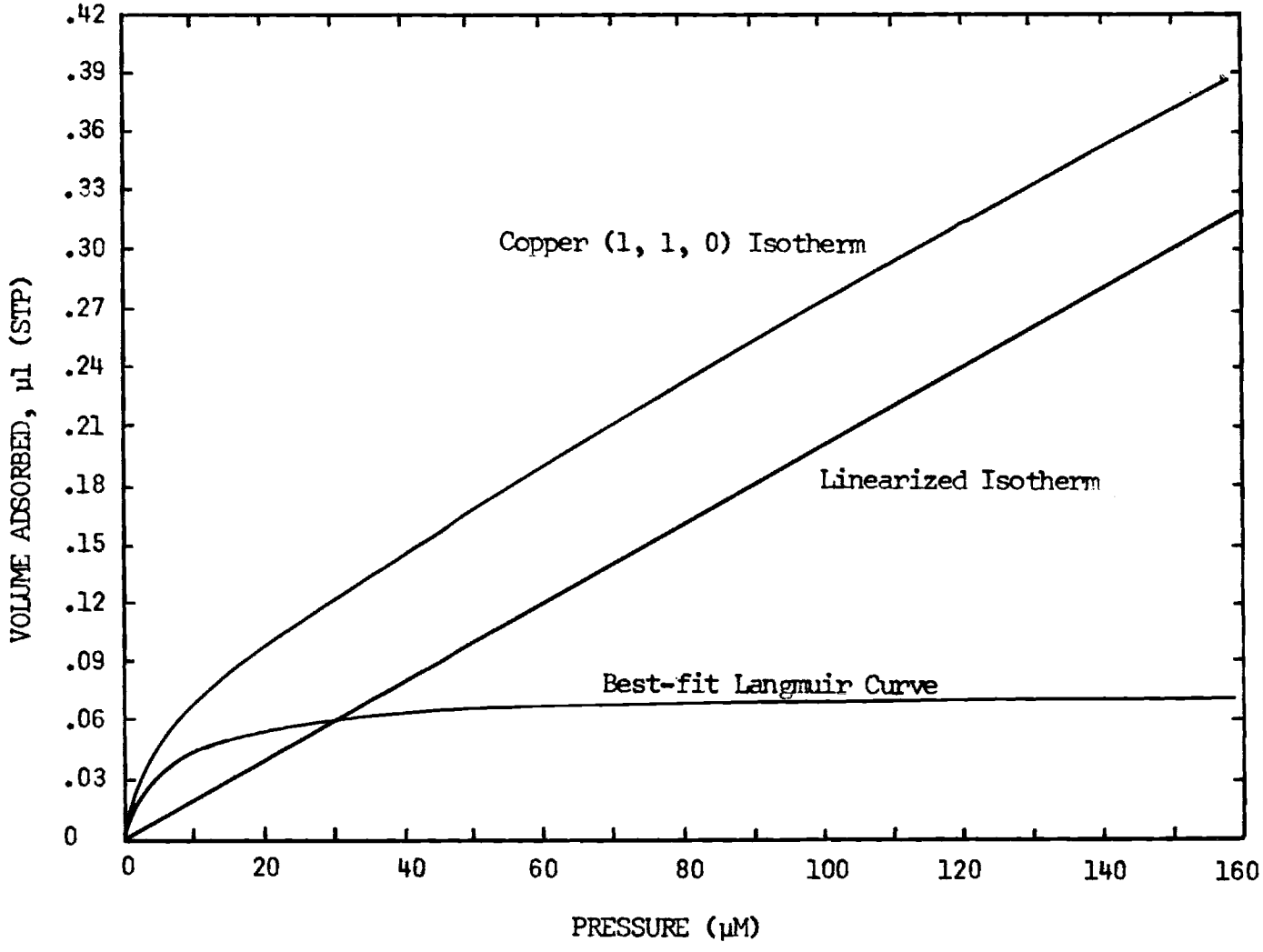

Figure 20. The Linearization of the 101.6° K Isotherm.

Table 7. Values of B_{2s}, n_m^h, and b

T(°K)	B_{2s}	n_m^h	b
72.8	506	--	--
79.9	36.6	--	--
92.2	4.64	0.101	1.15
101.6	0.573	0.0738	0.180
108.1	0.321	0.0753	0.163

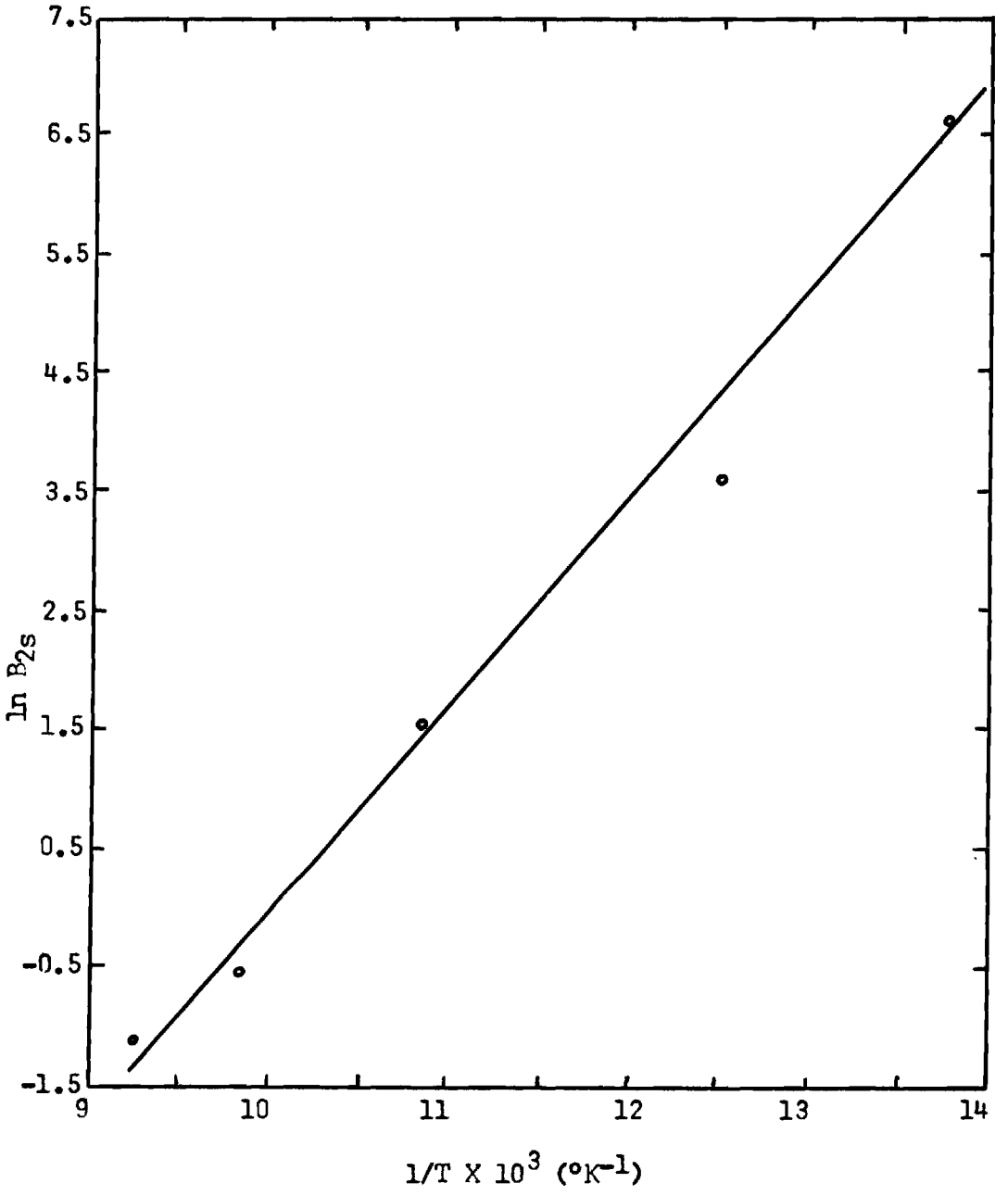

Figure 21. ln B_{2s} versus 1/T.

it was found that such changes would produce an error of 2-3% in the number of moles adsorbed on the crystals of copper. However, the individual isotherms could be reproduced to no better than about ±10% of the number of moles adsorbed. For this reason, the B_{2s} data on the copper-krypton isotherms is probably good to about 20%. Figure 22 presents a plot of $\ln B_{2s}$ vs 1/T, with the error bars accounting for the approximately 20% deviation allowed in the values of B_{2s}. The solid line corresponds to the best fit of equation (II-7) to the experimental data. Other reasonable lines drawn within the experimental error bars lead to the conclusion that the best fit value of ε'_{1s}/k could be too low by about 25°, or too high by about 100°K. The value of ε'_{1s}/k should then lie between the values of 1572° and 1698°K, the most likely value being about 1672°K.

Discussion

The cleaning procedure on the empty nickel cell indicated that much carbon was present on the nickel. This carbon is apparently not spread over the entire metal surface, but must be concentrated in very small areas (one possibility is that it is concentrated at grain boundaries). This conclusion is drawn because the krypton isotherms in figure 16 indicate a very strong interaction between the surface and krypton; it is even a stronger interaction than between krypton and the copper (1, 1, 0) crystals. On the other hand, the interaction of krypton with carbon is known to be much weaker than with copper.

Figure 23 compares the results of Carden's study on the (1, 1, 1) crystals with the present results on the (1, 1, 0) crystals. The slopes

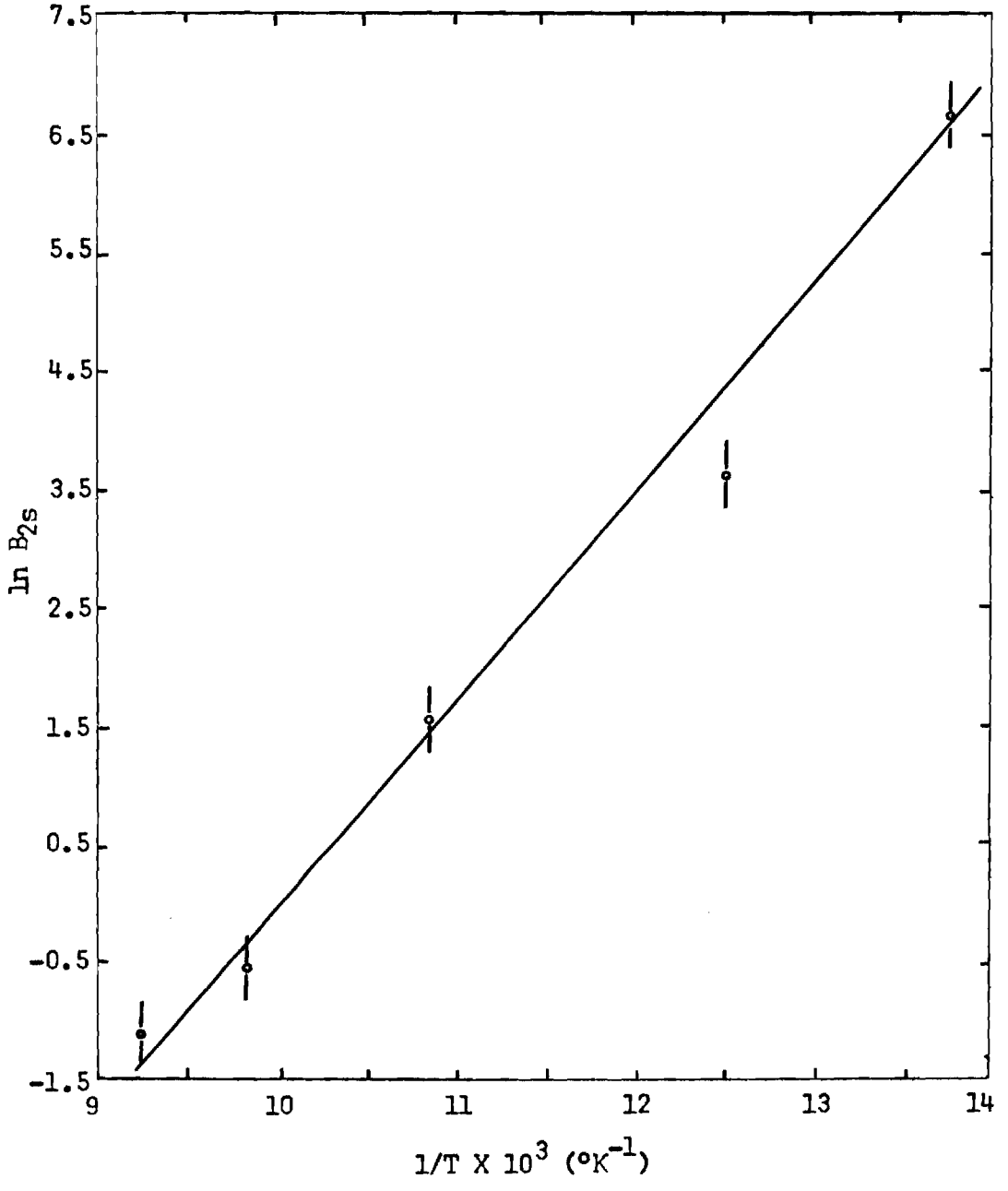

Figure 22. ln B_{2s} versus 1/T, Showing Limits of Experimental Error

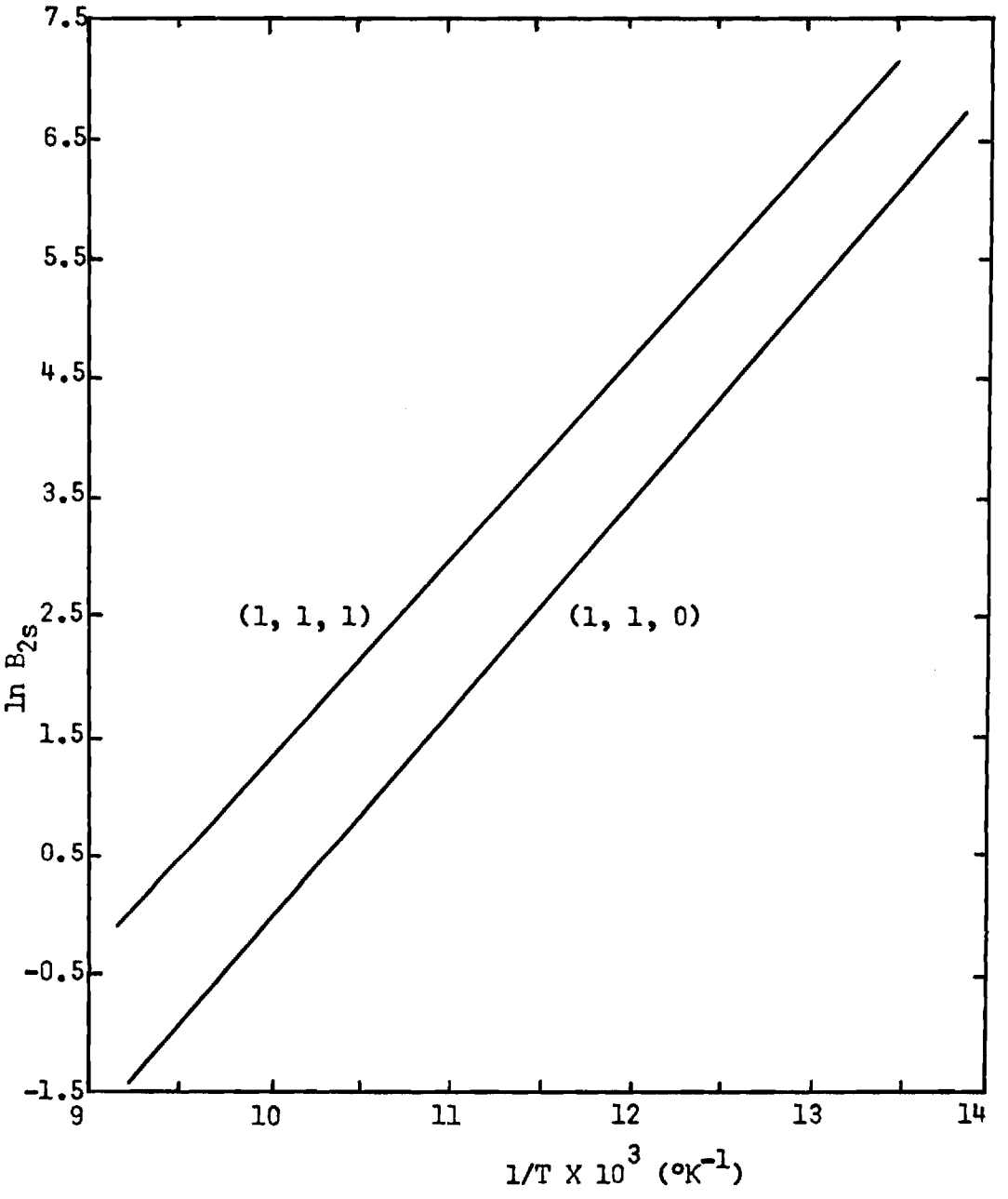

Figure 23. ln B_{2s} versus 1/T, Comparing Copper (1, 1, 1) and (1, 1, 0)

of the lines are related to the interaction parameters, ϵ'_{ls}/kT, while the vertical position of the lines is related to the surface area. The geometric area of Carden's crystals was lower than the crystals used in this study; 78 cm^2 as compared to 89 cm^2. Yet, the surface area as given by the virial analysis indicates a much lower area for the (1, 1, 0) crystals as compared to the (1, 1, 1) crystals because the best-fit line in figure 23 for the (1, 1, 0) crystals lies below the other line. The slopes are approximately equal, so that the interaction parameters are roughly equal. Quantitatively, if the value of Az_0 is divided by $z_0 = 3.4 \times 10^{-8}$ cm, then A is found to be 28 cm^2. The area that Carden found from his virial analysis was 49 cm^2.

The (1, 1, 0) surface thus appears to be similar to the model given in the introduction, where the metal was assumed to be a collection of 3.89 Å spheres spaced 2.55 Å apart. The potential curves given in figure 10 showed that some fraction of the (1, 1, 0) surface could interact with krypton as strongly as could the (1, 1, 1) surface. Since the sites of highest interaction should be selectively populated first, these are the sites that the low coverage virial analysis should find.

CHAPTER IV

CONCLUSIONS AND RECOMMENDATIONS FOR FURTHER STUDY

Conclusions

The interaction parameters ϵ'_{ls}/k and Az_0 have been obtained for the krypton-copper (1, 1, 0) system and were found to be 1672°K and 9.52×10^{-7} cm^3 respectively. These values seem to indicate, according to the lattice calculation presented in the introduction, that the view which considers the metal surface to be energetically homogeneous is inadequate, and that adsorption on the (1, 1, 0) surface is influenced by a variation of the adsorption potential within the surface plane. This is because the value of ϵ'_{ls}/k is larger than such theories predict; furthermore, the low value of Az_0 means that this particular energy is characteristic of only a small fraction of the surface. However, the magnitude of the experimental errors is such that this conclusion warrants further investigation.

Recommendations for Further Study

Various improvements could be made on the present equipment which would greatly improve the precision of the data. Probably the greatest experimental error is due to the operation of the cryostat, which causes large pressure fluctuations that far exceed the precision of the capacitance manometer. Thus it is not possible to take full advantage of the high precision of this instrument, because of temperature fluctuations

and changes in the liquid nitrogen level in the cryostat. It is recommended that proportional temperature and level controllers be installed on the cryostat.

Another source of error results in large temperature fluctuations in the vapor above the liquid nitrogen in the cryostat. This changes the temperature of the nickel tube which leads to the sample. The resulting pressure fluctuations could be reduced if the volume of the tube were reduced. Since the source of the high roughness factor found in the previous study was not due to an oxide film on the stainless steel tube, it is recommended that the nickel tube be replaced by a small diameter stainless steel tube.

Finally, the results of the lattice summation given in the introduction indicate that the krypton atoms may not be able to pass over the rows of copper atoms, since the energy barrier is larger than the thermal energy. From the geometry of the copper (1, 1, 0) surface, it can be seen that adsorbate atoms which occupy an effective area of 15.1 Å^2/molecule can just form a close packed structure and remain in registry with the copper surface. This packing density is the same as that found in bulk liquid krypton. Larger atoms would not be able to close pack, and would appear to occupy an unusually large area per molecule on the (1, 1, 0) surface. The question of whether the adsorbate atoms are constrained to move between rows of copper atoms might then be answered by observing the monolayer coverage of Xe atoms adsorbed on a copper (1, 1, 0) surface, and comparing this with the behavior of krypton.

Finally, Auger spectroscopy should be used to confirm that the cleaning procedure actually does result in a clean surface. Low energy electron diffraction should also be used to find out if the resulting surface has the (1, 1, 0) structure. With regard to the nickel cell, the cleaning procedure indicated gross contamination with carbon, and yet the krypton isotherms were indicative of a bare nickel surface. This point might be profitably investigated with scanning Auger spectroscopy.

APPENDIX A

Coefficients of Equation (I-101) Used to Represent the Molar Volume of Liquid Argon

Table 8. Coefficients of Equation (I-101) Used to Represent the Molar Volume of Liquid Argon*

Temperature °K	A_1 cm^3/gm mole	$A_2 \times 10^2$ cm^3/gm mole atm	$A_3 \times 10^5$ cm^3/gm mole atm^2
85	28.376544	-0.74713828	2.7431250
90	29.066305	-0.97441015	2.7430468
95	29.822848	-1.2016921	2.7431250
100	30.646175	-1.4289687	2.7431250
105	31.536285	-1.6562476	2.7431250
110	32.493169	-1.8835218	2.7431250
115	33.516860	-2.1108132	2.7431250
120	34.607303	-2.3380687	2.7431250
125	35.764544	-2.5653500	2.7431250
130	36.988576	-2.7926257	2.7430468
135	39.536852	-6.0946968	18.879609
140	41.755423	-7.1804382	18.879609
145	44.011321	-8.2661687	18.879531

* This table of values was taken from Mullins and Ziegler[1].

APPENDIX B

Reduced Potential Energy as a Function of Krypton Distance above a (1, 1, 1) and (1, 1, 0) Surface

Table 9. Reduced Potential Energy over Site a, Figure 9A.

z^*	U_k/ε
9.00	-0.881
7.00	-2.312
5.00	-7.664
4.50	-10.565
4.00	-13.728
3.80	-14.349
3.77	-14.351
3.75	-14.334
3.50	-12.174
3.30	-5.480
3.10	+11.19

* In tables 9-13, z is the distance between the krypton atom and a plane running through the centers of the surface atoms.

Table 10. Reduced Potential Energy over Site b, Figure 9A

z	Uk/ε
9.00	-0.881
5.00	-7.609
4.50	-10.480
4.00	-13.424
3.90	-13.703
3.85	-13.741
3.80	-13.686
3.70	-13.200
3.50	-9.65
3.30	+1.108

Table 11. Reduced Potential Energy over Site a, Figure 9B.

z	Uk/ε
9.00	-0.808
7.00	-2.005
6.00	-3.431
5.00	-6.272
4.50	-8.618
4.00	-11.621
3.80	-12.820
3.60	-13.735
3.55	-13.873
3.50	-13.957
3.45	-13.975
3.30	-13.471
3.10	-10.707
2.90	-3.442

Table 12. Reduced Potential Energy over Site b, Figure 9B

z	Uk/ε
9.00	-0.808
7.00	-2.005
6.00	-3.432
5.00	-6.273
4.50	-8.607
4.00	-11.538
3.80	-12.634
3.70	-13.060
3.60	-13.318
3.55	-13.363
3.50	-13.333
3.30	-12.080
3.10	-7.57

Table 13. Reduced Potential Energy over Site c, Figure 9B

z	Uk/ε
9.00	-0.808
7.00	-2.005
6.00	-3.433
5.00	-6.274
4.50	-8.553
4.00	-11.001
3.90	-11.300
3.80	-11.410
3.70	-11.230
3.50	-9.266
3.40	-6.920

APPENDIX C

Isotherm Data

Table 14. Isotherm Data at 72.8°K (Cell plus Copper (1, 1, 0) Crystals)

Equilibrium Pressure (μM-Hg)	Volume Adsorbed (μl-STP)
0.002	0.350
0.024	0.663
0.104	1.135
0.322	1.968
0.878	2.805
2.10	3.547
3.64	3.926
6.61	4.281
11.53	4.609
18.84	4.906
30.04	5.226
40.36	5.435
54.15	5.690
71.68	5.937
90.40	6.157
112.80	6.347
139.70	6.638
158.85	6.868
188.89	7.170

Table 14. (Continued)

Equilibrium Pressure (μM-Hg)	Volume Adsorbed (μl-STP)
217.98	7.507
252.87	8.027
284.59	8.463
319.93	8.692
355.72	9.378
395.36	10.355
441.62	10.840
487.82	11.353
531.38	11.763
571.78	13.163
589.73	13.550
608.09	14.280
626.34	17.110

Table 15. Isotherm Data at 79.9°K (Cell plus Copper (1, 1, 0) Crystals)

Equilibrium Pressure (μM-Hg)	Volume Adsorbed (μl-STP)
0.005	0.058
0.017	0.148
0.025	0.254
0.061	0.465
0.266	0.745
0.605	1.006
1.38	1.248
2.05	1.497
3.15	1.821
4.44	2.121
6.81	2.523
9.50	2.837
13.37	3.116
17.69	3.332
23.85	3.560
32.24	3.762
42.11	3.926
53.99	4.090
69.12	4.252

Table 15. (Continued)

Equilibrium Pressure (μM-Hg)	Volume Adsorbed (μl-STP)
88.58	4.421
114.03	4.596
144.75	4.785
180.64	4.969
225.19	5.152
291.87	5.403
372.93	5.659
472.24	5.878
596.25	6.128
695.04	6.301
769.19	6.430

Table 16. Isotherm Data at 92.2°K (Cell plus Copper (1, 1, 0) Crystals)

Equilibrium Pressure (μM-Hg)	Volume Adsorbed (μl-STP)
0.005	0.054
0.087	0.176
0.496	0.338
1.13	0.455
1.67	0.519
2.73	0.615
5.47	0.794
9.57	0.952
18.64	1.243
29.96	1.605
47.94	1.989
72.77	2.386
105.08	2.753
151.52	3.145
212.23	3.509
286.39	3.818
379.45	4.052
488.30	4.352
627.40	4.716

Table 17. Isotherm Data at 101.6°K (Cell plus Copper (1, 1, 0) Crystals)

Equilibrium Pressure (μM-Hg)	Volume Adsorbed (μl-STP)
0.014	0.024
0.097	0.077
0.235	0.114
0.681	0.172
1.87	0.255
4.98	0.362
8.89	0.441
17.71	0.552
32.56	0.686
63.55	0.890
98.98	1.115
154.81	1.403
233.05	1.783
331.34	2.056
447.50	2.414
554.29	2.612
671.05	2.800
757.71	2.870
840.06	3.109

Table 18. Isotherm Data at 108.1°K (Cell plus Copper (1, 1, 0) Crystals)

Equilibrium Pressure (μM-Hg)	Volume Adsorbed (μl-STP)
0.119	0.046
0.277	0.071
0.630	0.103
1.048	0.128
1.779	0.158
2.701	0.187
4.021	0.220
6.230	0.256
14.67	0.334
26.12	0.411
45.99	0.509
87.17	0.681
149.09	0.865
226.82	1.086
332.85	1.435
462.24	1.724
622.23	1.978
739.72	2.126
827.45	2.305

Table 19. Isotherm Data at 72.8°K (Empty Cell)

Equilibrium Pressure (μM-Hg)	Volume Adsorbed (μl-STP)
0.004	0.373
0.068	0.745
0.338	1.212
1.11	1.555
2.58	1.845
7.35	2.200
12.24	2.434
16.99	2.567
23.19	2.739
34.77	2.959
55.74	3.260
84.51	3.580
121.76	3.777
156.50	4.104
210.97	4.352
256.73	4.877
309.18	5.223
358.43	5.576
410.73	5.675

Table 19. (Continued)

Equilibrium Pressure (μM-Hg)	Volume Adsorbed (μl-STP)
468.73	6.353
522.13	7.162
580.64	8.578

Table 20. Isotherm Data at 79.9°K (Empty Cell)

Equilibrium Pressure (μM-Hg)	Volume Adsorbed (μl-STP)
0.025	0.295
0.228	0.576
0.879	0.850
1.83	1.121
3.84	1.329
7.03	1.508
12.01	1.683
21.46	1.886
32.62	2.042
46.48	2.207
68.45	2.395
90.05	2.543
120.89	2.680
157.23	2.897
203.63	3.059
257.73	3.269
321.64	3.447
395.46	3.661
478.32	3.841

Table 20. (Continued)

Equilibrium Pressure (μM-Hg)	Volume Adsorbed (μl-STP)
570.80	3.953
663.61	4.064
735.61	4.143

Table 21. Isotherm Data at 92.2°K (Empty Cell)

Equilibrium Pressure (μM-Hg)	Volume Adsorbed (μl-STP)
0.011	0.037
0.071	0.150
0.565	0.306
1.295	0.397
2.10	0.459
3.72	0.545
6.14	0.626
10.18	0.722
20.63	0.890
31.78	1.048
52.45	1.215
77.56	1.348
106.94	1.459
152.05	1.645
212.36	1.788
281.47	1.978
371.11	2.205
473.18	2.363
595.63	2.479
701.08	2.604

Table 22. Isotherm Data at 101.6°K (Empty Cell)

Equilibrium Pressure (μM-Hg)	Volume Adsorbed (μl-STP)
0.051	0.041
0.107	0.070
0.217	0.098
0.637	0.153
2.08	0.236
4.04	0.298
7.18	0.358
16.63	0.449
30.48	0.546
56.11	0.676
95.17	0.827
147.16	1.000
222.31	1.232
313.63	1.435
419.68	1.568
526.96	1.712
642.73	1.801
737.09	1.960
808.97	1.987

Table 23. Isotherm Data at 108.1°K (Empty Cell)

Equilibrium Pressure (μM-Hg)	Volume Adsorbed (μl-STP)
0.059	0.033
0.198	0.056
0.517	0.087
1.16	0.118
1.94	0.143
3.07	0.168
4.40	0.189
6.64	0.214
13.07	0.260
24.20	0.312
44.11	0.385
84.54	0.515
143.59	0.655
226.81	0.810
321.57	0.982
446.98	1.177
589.05	1.297
695.04	1.368

Table 24. Copper (1, 1, 0) Isotherm Data at 72.8°K

Equilibrium Pressure (μM-Hg)	Volume Adsorbed (μl-STP)
0.10	0.33
0.20	0.50
0.30	0.70
0.40	0.87
0.50	1.00
0.70	1.21
1.00	1.40
1.50	1.59
2.00	1.73
2.50	1.84
3.75	1.99
5.00	2.06
7.50	2.13
10.00	2.18
15.00	2.24
25.00	2.32
40	2.40
100	2.59
140	2.71

Table 24. (Continued)

Equilibrium Pressure (μM-Hg)	Volume Adsorbed (μl-STP)
180	2.89
220	3.02
260	3.24
300	3.60
340	4.04
380	4.48
420	4.76
460	4.85

Table 25. Copper (1, 1, 0) Isotherm Data at 79.9°K

Equilibrium Pressure (μM-Hg)	Volume Adsorbed (μl-STP)
1.00	0.20
1.50	0.26
2.00	0.34
2.50	0.43
3.00	0.53
3.50	0.62
4.00	0.70
5.00	0.83
6.00	0.95
7.50	1.09
10.00	1.26
15.0	1.48
20.0	1.58
30.0	1.69
40.0	1.76
60.0	1.84
80.0	1.88
100.0	1.91
160.0	1.97

Table 25. (Continued)

Equilibrium Pressure (μM-Hg)	Volume Adsorbed (μl-STP)
250	2.03
400	2.04
600	2.13

Table 26. Copper (1, 1, 0) Isotherm Data at 92.2°K

Equilibrium Pressure (μM-Hg)	Volume Adsorbed (μl-STP)
1.0	0.064
2.0	0.104
3.0	0.126
4.0	0.149
5.0	0.166
7.0	0.200
10.0	0.251
15.0	0.335
20.0	0.419
30.0	0.57
40.0	0.71
50.0	0.83
70.0	1.03
90.0	1.19
130.0	1.42
180.0	1.60
260	1.74
340	1.82
420	1.89

Table 26. (Continued)

Equilibrium Pressure (μM-Hg)	Volume Adsorbed (μl-STP)
500	1.98
580	2.07
660	2.18

Table 27. Copper (1, 1, 0) Isotherm Data at 101.6°K

Equilibrium Pressure (μM-Hg)	Volume Adsorbed (μl-STP)
1.0	0.018
2.0	0.029
5.0	0.045
10.0	0.069
15.0	0.083
20.0	0.098
30.0	0.123
45.0	0.155
65.0	0.200
100.0	0.276
140	0.345
200	0.448
260	0.528
340	0.640
420	0.739
500	0.825
580	0.901
660	0.968

Table 28. Copper (1, 1, 0) Isotherm Data at 108.1°K

Equilibrium Pressure (μM-Hg)	Volume Adsorbed (μl-STP)
1.0	0.013
2.0	0.022
3.0	0.031
4.0	0.037
6.0	0.044
10.0	0.055
15.0	0.067
20.0	0.078
30.0	0.097
40.0	0.111
60	0.132
100	0.184
180	0.281
260	0.361
340	0.434
420	0.495
500	0.546
580	0.597
660	0.645

BIBLIOGRAPHY

1. J. C. Mullins and W. T. Ziegler, Project A-764, Technical Report No. 3, Contract No. CST-1154, NBS, (1965).

2. J. E. Sinor and F. Kurata, J. Chem. Eng. Data, 11 (4), 537 (1966).

3. W. B. Streett, J. Chem. Phys., 42 (2), 500 (1965).

4. H. Volk and G. D. Halsey, Jr., J. Chem. Phys., 33 (4), 1132 (1960).

5. N. R. Kestner and O. Sinanoglu, J. Chem. Phys., 38 (7), 1730 (1963).

6. O. Sinanoglu, Chem. Phys. Letters, 1, 340 (1967).

7. K. Denbigh, "The Principles of Chemical Equilibrium", Cambridge University Press, London (1957).

8. T. L. Hill, "An Introduction to Statistical Thermodynamics", Addison-Wesley Publishing Company, Reading, Mass. (1960).

9. R. A. Pierotti and H. E. Thomas, Surf. and Coll. Science, Vol. IV, Wiley-Interscience, New York (1971).

10. T. L. Hill, J. Am. Chem. Soc., 79, 4885 (1957).

11a. R. A. Pierotti, Chem. Rev., 76, 717 (1976).

b. R. A. Pierotti and A. A. Liabastre, "The Structure and Properties of Water Solutions", Office of Water Resources, Research Project No. A-017-GA (1972).

12. R. H. Fowler and E. A. Guggenheim, "Statistical Thermodynamics", Cambridge University Press (1939).

13a. H. Reiss, H. L. Frisch, and J. L. Lebowitz, J. Chem. Phys., 31, 369 (1959).

b. H. Reiss, H. L. Frisch, E. Helfand, and J. L. Lebowitz, J. Chem. Phys., 32, 119 (1960).

c. H. Reiss and S. W. Mayer, J. Chem. Phys., 34, 2001 (1961).

d. H. L. Frisch, Adv. Chem. Phys., 6, 229 (1961).

e. H. Reiss, Adv. Chem. Phys., 9, 1 (1966).

f. J. L. Lebowitz, E. Helfand, and E. Praestgaard, J. Chem. Phys., 43, 774 (1965).

g. D. M. Tully-Smith and H. Reiss, J. Chem. Phys., 53, 4015 (1970).

h. S. J. Harris and D. M. Tully-Smith, J. Chem. Phys., 55, 1104 (1971).

i. H. Reiss and D. M. Tully-Smith, J. Chem. Phys., 1674 (1971).

j. H. Reiss and R. V. Casberg, J. Chem. Phys., 61, 1107 (1974).

14. J. O. Hirschfelder, C. F. Curtiss, and R. B. Bird, "Molecular Theory of Gases and Liquids", Wiley, New York (1967).

15. R. A. Pierotti, Chem. Phys. Letters, 2 (6), 385 (1968).

16. A. C. Levy, Ph. D. Thesis, Georgia Institute of Technology (1976).

17. J. L. Carden and R. A. Pierotti, J. Coll. and Int. Sci., 47 (2), 379 (1974).

18. J. L. Carden, Ph. D. Thesis, Georgia Institute of Technology (1972).

19. J. H. Kaspersma, Doctor's Thesis, Catholic University of Nijmegen, Netherlands (1972).

20. B. B. Fisher and W. G. McMillan, J. Chem. Phys., 62, 494 (1958).

21. F. W. Young, J. App. Phys., 32 (2), 192 (1961).

22. R. W. Powers, Electrochem. Tech., Sept.-Oct., 274 (1964).

23. J. J. McAlpin, Ph. D. Thesis, Georgia Institute of Technology (1966).

24. S. Brunauer, P. H. Emmett, and E. Teller, J. Am. Chem. Soc., 60, 309 (1938).

25. H. E. Thomas, R. N. Ramsey, and R. A. Pierotti, J. Chem. Phys., 59 (11), 6163 (1973).

26. G. A. Miller, J. Phys. Chem., 67, 1359 (1963).

VITA

Stephen Laurent Parrott was born May 3, 1949 in E. St. Louis, Illinois, the son of Barbara Jean Parrott and Cornelius Henry Parrott. He received his high school education in Jefferson City, Missouri, and in Atlanta, Georgia. He entered the Georgia Institute of Technology in September, 1967, and received a Bachelor of Science in Chemistry in June, 1972, and a Master of Science in Chemistry in August, 1973, by working under a special Surface Science and Technology program. At that time, he continued his graduate work at the Georgia Institute of Technology to study for the Doctor of Philosophy in the School of Chemistry.

He is married to the former Cheri' Suzon Lightsey, the daughter of Mr. and Mrs. Hiram Lightsey, of Baxley, Georgia.